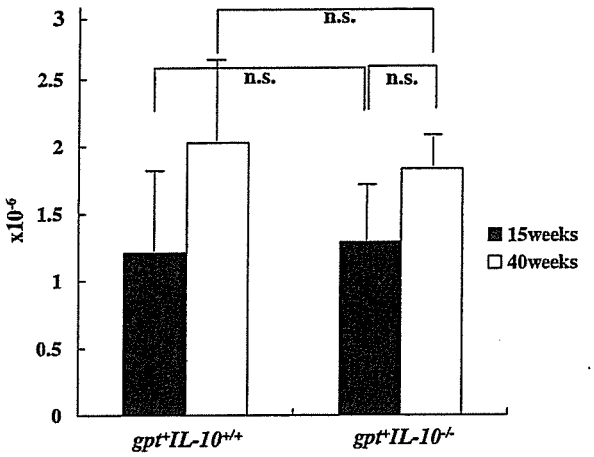

Fig. 4. Mutation frequency of Spi⁻ selection in the total colon of *gpt⁺IL-10⁻/⁻* mice and *gpt⁺IL-10⁺/⁺* mice (filled square, 15 weeks; unfilled square, 40 weeks). The mutation frequencies of Spi⁻ selection in the total colon of *gpt⁺IL-10⁻/⁻* mice were not significantly higher than those in the total colon of *gpt⁺IL-10⁺/⁺* mice, at 15 weeks or 40 weeks of age. The mutation frequencies of Spi⁻ selection in the total colon of 40-weeks *gpt⁺IL-10⁻/⁻* mice were not significantly higher than those in the total colon of 15-weeks *gpt⁺IL-10⁻/⁻* mice. $P < 0.05$, statistically significant difference versus *gpt⁺IL-10⁺/⁺*. Bars represent mean values and SE.

Table V. List of mutations in the colon (15 weeks, Spi⁻ selection)

gpt +IL-10⁻/⁻			*Gpt +IL-10 +/+*		
Position	Sequence change	Number	Position	Sequence change	Number
161~	-C	1	237	-C	1
164~	CCC→CC	1	238~	GGGG→GGG	1
226	-C	1	294	-G	1
227~	TTTTT→TTTT	2	295~	TTTTTT→TTTTT	2
235~250	-16 bp	1	327	-A	2
238~	GGGG→GGG	1	333~419	-87 bp	1
286~	CCCC→CCC	1	348~	CC→C	1
295~	TTTTTT→TTTTT	6	416~	TTTT→TTT	4
393~	CC→CCC	1			
416~	TTTT→TTT	2			

The position numbers indicate the locations where mutations were found. The numbering starts from the first nucleotide of the *gam* gene.

Table VI. List of mutations in the colon (40 weeks, Spi⁻ selection)

gpt +IL-10⁻/⁻			*gpt +IL-10 +/+*		
Position	Sequence change	Number	Position	Sequence change	Number
195~198	-TCTT	1	129	AA→A	1
227~	TTTTT→TTTT	5	227~	TTTTT→TTTT	3
232~	CC→C	3	232~	CC→C	1
238~	GGGG→GGG	2	286~	CCCC→CCC	3
277	-G	1	295~	TTTTTT→TTTTT	5
286~	CCCC→CCC	2	327	-A	1
295~	TTTTTT→TTTTT	4			
341	-T	1			

The position numbers indicate the locations where mutations were found. The numbering starts from the first nucleotide of the *gam* gene.

colon accumulate with time. Therefore, our data may reflect some mechanisms responsible for the p53 mutations of UC.

Microsatellite instability (MI) has been reported not only in colitic cancers but also in dysplasias and even in non-dysplastic inflamed mucosa, though the frequencies were not so great (4). It seems that MI is related to insufficient repair of replication errors. Transforming growth factor (TGF)-β1 inhibits the differentiation of some cells of mesodermal origin and potently inhibits the proliferation of epithelial cells. Conversely, cells that lose responsiveness to TGF-β1 may show uncontrolled growth and become tumorigenic. Previous studies showed that mutational inactivation of the polydeoxyadenine (poly A) microsatellite tract within *TGF-β1 receptor type II* (*TGF-β1RII*) occurs early and in a subset of UC neoplasms, and that the majority of reported mutations were 1- or 2-base deletions or insertions (15). In our study, small deletions and insertions had greatly increased, and ~90% of the 1 bp deletions and insertions occurred, just like microsatellite sequences and poly A tract, in the monotonous base runs or adjacent repeats of short tandem sequences. In a previous study on DNA polymerase δ, Fortune *et al.* (16) suggested that strand slippage during replication may be a primary source of insertion and deletion mutagenesis in eukaryotic genomes. Therefore, it may be suggested that the 1 bp deletions and insertions in the *gpt⁺IL-10⁻/⁻* mice increased because of a replication error following repeated mucosal injury and regeneration in the chronic inflammation.

Shin reported that the predominant spontaneous events observed in a mouse kidney epithelial cell line (K435) were G:C to C:G transversion mutations and small events observed in mutant cells isolated from the hydrogen peroxide and ionizing radiation exposed cells were also predominantly G:C to C:G transversions. They suggested that the mechanism did not include a classical deficiency in mismatch repair and the initial formation of C:C or G:G mispairs provided the most plausible explanation (17). At 15 weeks of age, the frequency of G:C to C:G in the colitis mice was most frequent and nine times higher than that of the control mice. The mutation mechanism, which did not include a classical deficiency in mismatch repair in the report on K435, may partially contribute to our data in *gpt⁺IL-10⁻/⁻* mice.

UC is a chronic inflammatory disease that produces reactive oxygen and nitrogen species and increases the risk of colorectal cancer. Reactive oxygen and nitrogen species produced by inflammatory cells can interact with key genes involved in carcinogenic pathways such as *p53*, DNA mismatch repair genes and even DNA base excision-repair genes (18,19). In previous studies, a positive correlation was observed between higher inducible nitric oxide synthase (iNOS) activity and increased *p53* G:C to A:T transitions in inflamed colon and colon cancer (11,14). The deamination of 5-methylcytosine has been argued to be a major mechanism for the induction of G:C to A:T transitions at CpG dinucleotides in DNA (20). Nitric oxide produced during inflammation may cause both deamination and oxidative damage to DNA. It has been reported that *IL-10⁻/⁻* mice had increased damage scores and granulocyte infiltration concurrent with increased mRNA and protein synthesis for iNOS in intestinal tissues (21). These data suggest that oxidative stress and DNA adducts may drive the accumulation of mutations in the colon of the *gpt⁺IL10⁻/⁻* mice. In a previous paper on chronic *Helicobacter pylori* infections, it was suggested that the Helicobacter-infected mice exhibited severe gastritis and a high level of

iNOS messenger RNA expression and A:T to C:G and G:C to T:A transversions had greatly increased (22). In our study, the frequency of G:C to T:A transversions in the 40-weeks *gpt*$^{+}$*IL-10*$^{-/-}$ mice was 2.6 times higher than that of the 40-weeks control mice, and 3.3 times higher than that of the 15-weeks *gpt*$^{+}$*IL-10*$^{-/-}$ mice. On this point, the mutation spectrum of our result was similar to that of the paper on chronic *Helicobacter pylori* infections. On the contrary, our data suggested that G:C to A:T transitions in the inflamed colon accumulate with time unlike that suggested in the paper on chronic *Helicobacter pylori* infections. We think that the difference between our result and the paper on chronic *Helicobacter pylori* infections is due to differences of organs, duration of inflammation or methods of mutation assay.

It was necessary to confirm that the mutant frequency in non-inflamed organs of *IL10*$^{-/-}$ mice did not increase. We analyzed livers in the 40-weeks mice as non-inflamed organ in order to clear whether the effect observed is associated to inflammation or IL-10 deficiency. At 40 weeks of age, the 6-TG mutant frequency in the liver of the *gpt*$^{+}$*IL10*$^{-/-}$ mice was 2.4×10^{-6}, which was not significantly different from the *gpt*$^{+}$*IL10*$^{+/+}$ mice (1.7×10^{-6}). The livers of the *gpt*$^{+}$*IL10*$^{-/-}$ mice were not inflamed, macroscopically. In consequence, it was suggested that the effect observed was associated to inflammation.

In our data, several types of mutations increased, and it is suggested that multiple mechanisms have a role in carcinogenesis of inflamed colon. In the mutations of the *gpt*$^{+}$*IL10*$^{-/-}$ mice, short deletions or insertions in the monotonous base runs or adjacent repeats of short tandem sequences and G:C to A:T transitions were striking mutations. Therefore, biochemical support may be useful for proving that replication error and oxidative stress mainly play a role in carcinogenesis in the inflamed colon.

Acknowledgements

We are deeply grateful to Prof. Tetsuya Ono for his appropriate advices on mouse experiments. This work was supported in part by a grant-in-aid from the Japan Society for the Promotion of Science, and by the Kurokawa Cancer Foundation.

Conflict of Interest Statement: None declared.

References

1. Sugita,A., Sachar,D.B., Bodian,C., Ribeiro,M.B., Aufses,A.H.Jr. and Greenstein,A.J. (1991) Colorectal cancer in ulcerative colitis. Influence of anatomical extent and age at onset on colitis-cancer interval. *Gut*, **32**, 167–169.
2. Kern,S.E., Redston,M., Seymour,A.B., Caldas,C., Powell,S.M., Kornacki,S. and Kinzler,K.W. (1994) Molecular genetic profiles of colitis-associated neoplasms. *Gastroenterology*, **107**, 420–428.
3. Willenbucher,R.F., Aust,D.E., Chang,C.G., Zelman,S.J., Ferrell,L.D., Moore,D.H.II and Waldman,F.M. (1999) Genomic instability is an early event during the progression pathway of ulcerative-colitis-related neoplasia. *Am. J. Pathol.*, **154**, 1825–1830.
4. Takahashi,S., Kojima,Y., Kinouchi,Y., Negoro,K., Takagi,S., Aihara,H., Obana,N., Matsumoto,K., Hiwatashi,N. and Shimosegawa,T. (2003) Microsatellite instability and loss of heterozygosity in the nondysplastic colonic epithelium of ulcerative colitis. *J. Gastroenterol.*, **38**, 734–739.
5. Berg,D.J., Davidson,N., Kuhn,R., Muller,W., Menon,S., Holland,G., Thompson-Snipes,L., Leach,M.W. and Rennick,D. (1996) Enterocolitis and colon cancer in interleukin-10-deficient mice are associated with aberrant cytokine production and CD4(+) TH1-like responses. *J. Clin. Invest.*, **98**, 1010–1020.
6. Masumura,K., Matsui,M., Katoh,M., Horiya,N., Ueda,O., Tanabe,H., Yamada,M., Suzuki,H., Sofuni,T. and Nohmi,T. (1999) Spectra of gpt mutations in ethylnitrosourea-treated and untreated transgenic mice. *Environ. Mol. Mutagen.*, **34**, 1–8.
7. Takeiri,A., Mishima,M., Tanaka,K., Shioda,A., Ueda,O., Suzuki,H., Inoue,M., Masumura,K. and Nohmi,T. (2003) Molecular characterization of mitomycin C-induced large deletions and tandem-base substitutions in the bone marrow of gpt delta transgenic mice. *Chem. Res. Toxicol.*, **16**, 171–179.
8. Miyaki,M., Konishi,M., Kikuchi-Yanoshita,R. *et al.* (1994) Characteristics of somatic mutation of the adenomatous polyposis coli gene in colorectal tumors. *Cancer Res.*, **54**, 3011–3020.
9. Redston,M.S., Papadopoulos,N., Caldas,C., Kinzler,K.W. and Kern,S.E. (1995) Common occurrence of APC and K-ras gene mutations in the spectrum of colitis-associated neoplasias. *Gastroenterology*, **108**, 383–392.
10. O'Riordan,A. and Shanahan,F. (2001) p53 at the crossroads of colitis and cancer. *Gastroenterology*, **120**, 1877–1878.
11. Hussain,S.P., Amstad,P., Raja,K. *et al.* (2000) Increased p53 mutation load in noncancerous colon tissue from ulcerative colitis: a cancer-prone chronic inflammatory disease. *Cancer Res.*, **60**, 3333–3337.
12. Noffsinger,A.E., Belli,J.M., Miller,M.A. and Fenoglio-Preiser,C.M. (2001) A unique basal pattern of p53 expression in ulcerative colitis is associated with mutation in the p53 gene. *Histopathology*, **39**, 482–492.
13. Yoshida,T., Mikami,T., Mitomi,H. and Okayasu,I. (2003) Diverse p53 alterations in ulcerative colitis-associated low-grade dysplasia: full-length gene sequencing in microdissected single crypts. *J. Pathol.*, **199**, 166–175.
14. Goodman,J.E., Hofseth,L.J., Hussain,S.P. and Harris,C.C. (2004) Nitric oxide and p53 in cancer-prone chronic inflammation and oxyradical overload disease. *Environ. Mol. Mutagen.*, **44**, 3–9.
15. Souza,R.F., Lei,J., Yin,J. *et al.* (1997) A transforming growth factor beta 1 receptor type II mutation in ulcerative colitis-associated neoplasms. *Gastroenterology*, **112**, 40–45.
16. Fortune,J.M., Pavlov,Y.I., Welch,C.M., Johansson,E., Burgers,P.M. and Kunkel,T.A. (2005) Saccharomyces cerevisiae DNA polymerase delta: high fidelity for base substitutions but lower fidelity for single- and multi-base deletions. *J. Biol. Chem.*, **280**, 29980–29987.
17. Shin,C.Y., Ponomareva,O.N., Connolly,L. and Turker,M.S. (2002) A mouse kidney cell line with a G:C –> C:G transversion mutator phenotype. *Mutat. Res.*, **503**, 69–76.
18. Chang,C.L., Marra,G., Chauhan,D.P., Ha,H.T., Chang,D.K., Ricciardiello,L., Randolph,A., Carethers,J.M. and Boland,C.R. (2002) Oxidative stress inactivates the human DNA mismatch repair system. *Am. J. Physiol. Cell. Physiol.*, **283**, C148–C154.
19. Hofseth,L.J., Khan,M.A., Ambrose,M. *et al.* (2003) The adaptive imbalance in base excision-repair enzymes generates microsatellite instability in chronic inflammation. *J. Clin. Invest.*, **112**, 1887–1894.
20. Kreutzer,D.A. and Essigmann,J.M. (1998) Oxidized, deaminated cytosines are a source of C –> T transitions in vivo. *Proc. Natl Acad. Sci. USA*, **95**, 3578–3582.
21. Popoff,I., Jijon,H., Monia,B., Tavernini,M., Ma,M., McKay,R. and Madsen,K. (2002) Antisense oligonucleotides to poly(ADP-ribose) polymerase-2 ameliorate colitis in interleukin-10-deficient mice. *J. Pharmacol. Exp. Ther.*, **303**, 1145–1154.
22. Touati,E., Michel,V., Thiberge,J.M., Wuscher,N., Huerre,M. and Labigne,A. (2003) Chronic Helicobacter pylori infections induce gastric mutations in mice. *Gastroenterology*, **124**, 1408–1419.

Received July 29, 2005; revised September 5, 2005; accepted December 20, 2005

Environmental and Molecular Mutagenesis 47:277–283 (2006)

In Vivo Mutagenesis in the Lungs of *gpt*-delta Transgenic Mice Treated Intratracheally With 1,6-Dinitropyrene

Akiko H. Hashimoto,[1] Kimiko Amanuma,[1] Kyoko Hiyoshi,[1,2] Hirohisa Takano,[1] Ken-ichi Masumura,[3] Takehiko Nohmi,[3] and Yasunobu Aoki[1]*

[1]*Research Center for Environmental Risk, National Institute for Environmental Studies, Ibaraki, Japan*

[2]*Graduate School of Comprehensive Human Sciences, University of Tsukuba, Ibaraki, Japan*

[3]*Division of Genetics and Mutagenesis, National Institute of Health Sciences, Tokyo, Japan*

1,6-Dinitropyrene (1,6-DNP) is a ubiquitous airborne pollutant found in diesel exhaust. In this study, mutagenesis was examined in the lungs of *gpt*-delta transgenic mice after intratracheal instillation of 0–0.1 mg 1,6-DNP. In addition, the 1,6-DNP-induced *gpt* mutation spectrum was compared with that of control mice. A single intratracheal injection of 0–0.05 mg 1,6-DNP resulted in significant dose-dependent increases in mutant frequency; the induced mutant frequency declined at the 0.1 mg dose. The average lung mutant frequencies at doses of 0.025, 0.05, and 0.1 mg 1,6-DNP were 2.9-, 4.1-, and 1.9-times higher than for control mice ($(0.50 \pm 0.16) \times 10^{-5}$). The major mutations induced by 1,6-DNP included G:C→A:T transitions, G:C→T:A transversions, and 1-base deletions. Among the G:C→A:T transitions isolated from 1,6-DNP-treated mice, five (at nucleotide positions 64, 110, 115, 116, and 418) were observed in four or more animals. These positions therefore are potential hotspots for 1,6-DNP mutation. The predominant frameshift mutations following 1,6-DNP treatment included single base pair deletions at G:C (9/13 = 69%). The results of this study indicate that 1,6-DNP is mutagenic for the lungs of mice. Environ. Mol. Mutagen. 47:277–283, 2006.

Key words: 1,6-dinitropyrene; *gpt*-delta transgenic mouse; 6-thioguanine selection

INTRODUCTION

Suspended particulate matter in diesel exhaust (DE) is a suspected cause of lung cancer and allergic respiratory disease, including bronchial asthma [Muranaka et al., 1986]. Various potent carcinogens and mutagens, such as polycyclic aromatic hydrocarbons (PAHs) and nitrated PAHs, have been identified in DE particles [Harris, 1983]. Some of the compounds in DE, for instance, benzo[*a*]pyrene (B[*a*]P) and dinitropyrenes (DNPs), are pulmonary carcinogens in animals [Tokiwa et al., 1984; Brightwell et al., 1986; Jeffrey et al., 1990]. Among the DNPs, 1,6-DNP-induced lung tumors were detected in 50% of BALB/c mice after 112 days of s.c. inoculation [Tokiwa et al., 1984]. Following intratracheal instillation of 1,6-DNP, 90–100% of hamsters developed lung carcinomas along with myeloid leukemias [Takayama et al., 1985]. Iwagawa et al. [1989] showed that direct pulmonary instillation of 1,6-DNP led to lung tumors in Fischer 344 rats, and mutations in K-*ras* codon 12 were observed in the tumors induced in rat lungs using a similar dosing protocol [Smith et al., 1997]. Also, DNA adduct formation and gene mutation were analyzed in F344 rats in which 1,6-DNP was directly administered to the lungs by implantation. A significant increase in *Hprt* gene mutations was detected in spleen T-lymphocytes [Smith et al., 1995].

Earlier in vitro assay results indicated that DNPs are potent mutagens. In the Salmonella mutation assay (Ames test), DNPs display strong mutagenicity without an exogenous metabolic activation system and predominantly induce frameshift-type mutations [Mermelstein et al., 1981; Sugimura and Takayama, 1983; Tokiwa et al.,

Grant sponsor: Japan Society for the Promotion of Sciences; Grant Number: 14207100.

*Correspondence to: Yasunobu Aoki, National Institute for Environmental Studies, 16-2 Onogawa, Tsukuba, Ibaraki 305-8506, Japan. E-mail: ybaoki@nies.go.jp

Received 22 September 2005; provisionally accepted 7 October 2005; and in final form 6 January 2006

DOI 10.1002/em.20204

Published online 17 February 2006 in Wiley InterScience (www.interscience.wiley.com).

1984]. Salmeen et al. [1984] showed that mono- and dinitro-PAHs, which include 1,3-, 1,6-, and 1,8-DNP, 1-nitropyrene, and 3- and 8-nitrofluoranthene, account for 30–40% of the direct bacterial mutagenic activity of extracts from DE particulate. 1,6-DNP and 1,8-DNP are activated by nitroreduction and *O*-acetylation in bacteria to form DNA adducts [Rosenkranz and Mermelstein, 1983]. Following a single i.p. injection of 1,6-DNP into mice, this mutagen binds to lung DNA as 1-*N*-(deoxyguanosin-8-yl) amino-6-nitropyrene [Delclos et al., 1987]. The same guanine adduct also was formed in rat lungs instilled with 1,6-DNP [Smith et al., 1995]. The in vivo mutagenicity and mutation spectrum of 1,6-DNP in the lung, a target organ for air pollutants, should be useful for elucidating its carcinogenic mechanism of action. Oral administration of 1,3-, 1,6-, and 1,8-DNP mixtures leads to in vivo mutagenicity in MutaMouse® [Kohara et al., 2002]. However, the mutagenic effects of 1,6-DNP in the lung remain to be determined.

To estimate the in vivo mutagenicity of 1,6-DNP in the lung, we used the *gpt*-delta transgenic mouse [Nohmi et al., 1996; Thybaud et al., 2003]. These mice carry a λ phage EG10 transgene that includes the guanine phosphoribosyltransferase (*gpt*) gene. When the rescued phages are infected into *E. coli* expressing Cre recombinase, phage DNA is converted into plasmids harboring a gene for chloramphenicol (Cm) resistance (*cat*) and the *gpt* gene. The *gpt* mutants are detected as colonies arising on plates containing Cm and 6-thioguanine (6-TG). In this study, the mutant frequency and mutation spectrum obtained from the lungs of *gpt*-delta mice were examined after intratracheal instillation of 1,6-DNP. Mutant frequency in the lung increased in the presence of 0-0.05 mg 1,6-DNP. The predominant mutations induced by 1,6-DNP were G:C→A:T transitions, G:C→T:A transversions, and single-base deletions at C:G sites. Specifically, *gpt* nucleotides no. 64, 110, 115, 116, and 418 appeared to be mutation hotspots.

MATERIALS AND METHODS

Treatment of Mice

Twelve male *gpt*-delta mice were obtained from Japan SLC (Shizuoka, Japan). These mice carry about 80 copies of λ EG10 DNA on chromosome 17 in a C57BL/6J background [Nohmi et al., 1996]. Doses of 1,6-DNP (Sigma–Aldrich Japan, Tokyo, Japan) dissolved in tricaprylin {$[CH_3(CH_2)_6COOCH_2]_2CHOCO(CH_2)_6CH_3$} (Sigma–Aldrich, St Louis, MO) were administered to each of three 9-week-old mice via a single intratracheal instillation. The animals were anesthetized with 4% halothane (Hoechst Japan, Tokyo, Japan) until the animal did not respond to a tactile stimulus. The animal was placed on a restraining board with linen threads to hold the mouth open. The 1,6-DNP solution was instilled into the trachea via a polyethylene tube [Takano et al., 2002; Hashimoto et al., 2005]. Two doses (0.025 and 0.05 mg) of 1,6-DNP were dissolved in 50 μl tricaprylin, while the 0.1 mg dose was dissolved in 100 μl tricaprylin. Three mice were treated with 50 μl tricaprylin alone as controls. Mice were killed 14 days after 1,6-DNP treatment, which a previous study [Suzuki et al., 1999] indicated was sufficient for mutant manifestation in the lung. Their lungs were removed, frozen in liquid nitrogen, and stored at −80°C until DNA isolation.

gpt Mutation Assay

The *gpt* assay was performed as described previously [Nohmi et al., 2000]. High molecular weight genomic DNA was extracted from the pooled lung tissue from each animal, using the RecoverEase DNA isolation kit (Stratagene, La Jolla, CA). λ EG10 phages were rescued using Transpack packaging extract (Stratagene). To convert phage DNA into plasmids, *E. coli* YG6020 expressing Cre recombinase was infected with phage. Bacteria were spread onto M9 salt plates containing Cm and 6-TG [Nohmi et al., 2000], and incubated for 72 hr at 37°C for selection of colonies harboring a plasmid carrying the Cm acetyltransferase (*cat*) gene and a mutated *gpt* gene. The 6-TG–resistant colonies were streaked onto selection plates for confirmation of the resistant phenotype. Cells were cultured in LB broth containing 25 μg/ml Cm at 37°C and collected by centrifugation. Bacterial pellets were stored at −80°C until sequencing analysis.

PCR and DNA Sequence Analysis of 6-TG-mutants

A 739-bp DNA fragment containing the *gpt* gene was amplified by PCR using primer-1 and primer-2, as described previously [Nohmi et al., 2000; Hashimoto et al., 2005]. The reaction mixture contained 5 pmol of each primer, and was 200 mM for each dNTP. PCR was performed using Ex *Taq* DNA polymerase (Takara Bio, Shiga, Japan) with a PTC-100 Thermal Cycler (MJ Research, Waltham, MA). The reaction mixture was incubated at 94°C for 4.5 min, followed by 30 cycles of 30 sec at 94°C, 30 sec at 58°C, and 1 min at 72°C. The last step was extended for 5 min at 72°C. After purification, amplified products were sequenced with a Big Dye Terminator v3.1 Cycle sequencing kit (Applied Biosystems, Foster City, CA) and an Applied Biosystems model 3730xl DNA analyzer. The sequencing oligonucleotides, primer-A and primer-C, are given in earlier reports [Nohmi et al., 2000; Hashimoto et al., 2005].

Statistical Analysis

All data are expressed as mean ± SD. The statistical significance of the mutant frequency data was analyzed using ANOVA and the Tukey post-hoc test. Data were considered statistically significant at $P < 0.05$. To evaluate the mutant frequency dose response, simple linear regression was performed. Mutational spectra were compared using the Adams–Skopek test [Adams and Skopek, 1987; Cariello et al., 1994].

RESULTS

1,6-DNP-Induced *gpt* Mutations in the Lung

To examine the mutagenic effects of 1,6-DNP in the lung, *gpt*-delta transgenic mice were exposed to increasing doses of 1,6-DNP (0.025, 0.05, and 0.1 mg/mouse) by intratracheal instillation (Fig. 1). The mutant frequency in the lungs of control mice was $(0.5 \pm 0.2) \times 10^{-5}$ (Table I). The mutant frequencies in control mice in this study were similar to those observed previously in several tissues of *gpt*-delta mice [Masumura et al., 1999, 2000, 2003; Hashimoto et al., 2005]. Single injections of 0.025, 0.05, and 0.1 mg 1,6-DNP resulted in 2.9-, 4.1-, and 1.9-

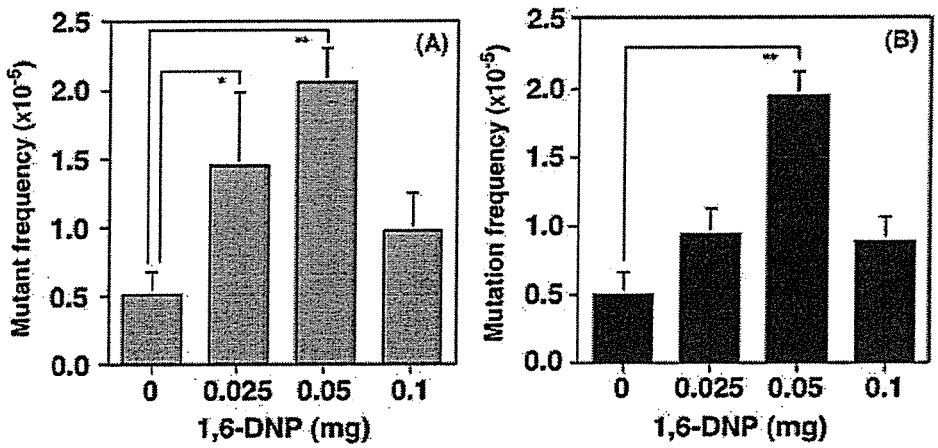

Fig. 1. 6-TG–resistant mutant frequency (A) and mutation frequency (B) in 1,6-DNP-treated *gpt*-delta mice. Data are presented as mean ± SD. Statistical significance was determined using ANOVA and Tukey tests. Significant differences between control and 1,6-DNP-induced groups are indicated (*$P < 0.05$, **$P < 0.01$).

TABLE I. Summary of Mutant and Mutation Frequencies in the Lungs of *gpt*-delta Mice After 1,6-DNP Treatment[a]

1,6-DNP amount (mg)	ID of animals	Number of colonies: Mutant	Number of colonies: Total	Mutant frequency (10^{-5})	Average mutant frequency ± SD (10^{-5})	% independent mutations	Mutation frequency (10^{-5})	Average mutation frequency ± SD (10^{-5})
Control	1	3	441,600	0.68		100	0.68	
	2	3	643,200	0.47		100	0.47	
	3	3	828,000	0.36		100	0.36	
	Total	*9*	*1,912,800*		*0.50 ± 0.16*			*0.50 ± 0.16*
0.025	1	7	608,000	1.15		83	0.96	
	2	9	800,000	1.13		67	0.75	
	3	13	630,400	2.06		54	1.11	
	Total	*29*	*2,038,400*		*1.45 ± 0.53*[b]			*0.94 ± 0.18*
0.05	1	15	652,800	2.30		91	2.10	
	2	9	502,400	1.79		100	1.79	
	3	14	678,400	2.06		91	1.88	
	Total	*38*	*1,833,600*		*2.05 ± 0.25*[c]			*1.92 ± 0.15*[c]
0.1	1	12	953,600	1.26		83	1.05	
	2	7	1,000,000	0.70		100	0.70	
	3	5	536,000	0.93		100	0.93	
	Total	*24*	*2,489,600*		*0.96 ± 0.28*			*0.89 ± 0.18*

[a]Statistical significance was determined using ANOVA test and Tukey test. Significant differences between the control and 1,6-DNP treated groups are indicated.
[b]$P < 0.05$.
[c]$P < 0.01$.

fold increases in mutant frequency ($(1.5 \pm 0.5) \times 10^{-5}$, $(2.1 \pm 0.3) \times 10^{-5}$, and $(1.0 \pm 0.3) \times 10^{-5}$) and 1.9-, 3.8-, and 1.8-fold increases in mutation frequency ($(0.9 \pm 0.2) \times 10^{-5}$, $(1.9 \pm 0.2) \times 10^{-5}$, and $(0.9 \pm 0.2) \times 10^{-5}$), compared with that in control mice, respectively. Mutant frequency was significantly increased at doses of 0.025 and 0.05 mg 1,6-DNP, but not at a dose of 0.1 mg 1,6-DNP. The mutation frequencies in these mice, calculated by correcting the mutant frequencies for the independence of the mutants determined by DNA sequencing (see below), are also shown in Table I and Figure 1.

Characteristics of the *gpt* Mutant Spectrum in 1,6-DNP-Treated Mice

To determine the mutation spectrum induced by 1,6-DNP in the lung, 99 *gpt* mutants from the lungs of treated and control mice were subjected to DNA sequencing analysis (Table II, Fig. 2). G:C→A:T transitions, G:C→T:A transversions, and 1-base deletions were the major mutations induced by 1,6-DNP as shown in Figure 2, which shows the mutant frequency in the treatment groups associated with each type of mutation. In the 1,6-DNP treated group, 47% of the mutations (36 out of 77 mutants) were

TABLE II. Classification of *gpt* Mutations From the Lungs of Control and 1,6-DNP-Treated Mice[a]

Type of mutation in the *gpt* gene	Control[b]		1,6-DNP total[c]		1,6-DNP (mg)					
					0.025		0.05		0.1	
	Total/ independent	%/% independent	Total/ independent	%/% independent	Total/ independent	%/% independent	Total/ independent	%/% independent	Total/ independent	%/% independent
Base substitution										
Transition										
G:C→A:T (CpG site)	10/10 (3/3)	45/48	36/27 (21/13)	47/43	13/7 (9/4)	46/39	13/12 (6/5)	46/46	10/8 (6/4)	48/42
A:T→G:C	2/2	9/10	6/5	8/8	3/2	11/11	1/1	4/4	2/2	10/11
Transversion										
G:C→T:A	4/4	18/19	13/11	17/17	6/4	21/22	5/5	18/19	2/2	10/11
G:C→C:G	4/3	18/14	3/3	4/5	0	0	1/1	4/4	2/2	10/11
A:T→T:A	0	0	1/1	1/2	1/1	4/6	0	0	0	0
A:T→C:G	0	0	2/2	3/3	1/1	4/6	0	0	1/1	5/5
Deletion										
1-base	2/2	9/10	13/12	17/19	2/2	7/11	7/6	25/23	4/4	19/21
Insertion	0	0	3/2	4/3	2/1	7/6	1/1	4/4	0	0
Total	*22/21*	*100*	*77/63*	*100*	*28/18*	*100*	*28/26*	*100*	*21/19*	*100*

[a]Independent mutations were isolated no more than once from any individual mouse.
[b]Control mutations are the sum of the mutations obtained from control animals in this study plus the mutations obtained from control animals in a previous study [Hashimoto et al., 2005]. The numbers of each type of mutation in control animals from this study were obtained from Table III.
[c]Mutations combined from all treatment doses.

G:C→A:T transitions, while 17% (13/77) were G:C→T:A transversions together with an equal percentage of 1-base deletions. In control mice, 78% (7/9) of the total mutations were G:C→A:T transitions. To increase the number of control mutants used for comparison, 9 mutants from this study were combined with 13 control lung mutants isolated from a previous study performed analogously to this one [Hashimoto et al., 2005], and this pooled mutant spectrum is used for the data shown in Table II and the mutant frequency distribution shown in Figure 2. There were no significant differences between spectra of the 22 control mutations and 77 total 1,6-DNP-induced mutations (Table II) ($P = 0.39$, Adams–Skopek test).

The *gpt* mutations isolated from 1,6-DNP-treated mice are listed in Table III. Among the G:C→A:T transitions isolated from treated mice, five (at nucleotides 64, 110, 115, 116, and 418) were observed in four or more mice. These positions are therefore potential hotspots for 1,6-DNP mutations; however, no significant differences were observed between the positions of the control mutations isolated in this study and the positions of the 1,6-DNP mutations ($P = 0.61$, Adams–Skopek test). There were also no significant differences between the positions of the 22 control lung mutations pooled from this study and our previous study [Hashimoto et al., 2005] and the 77 1,6-DNP-induced mutations ($P = 0.08$, Adams–Skopek test). The predominant frameshift mutation after 1,6-DNP treatment was single base-pair deletions at G:C (9/13 = 69%). Seventy-seven percent of 1-base deletions (10/13) occurred in run sequences, and there were no hotspots for 1-base deletions.

DISCUSSION

DNPs are recognized as potent environmental mutagens. Moreover, 1,6-DNP is a carcinogen in experimental animals [Tokiwa et al., 1984]. Using the Ames test, 43% of the direct mutagenicity of diesel particulate extracts was estimated to be due to contaminant DNPs [Nakagawa et al., 1983]. A 1,3-, 1,6-, and 1,8-DNP mixture was mutagenic in the liver, lung, colon, stomach, and bone marrow after intragastric injection in MutaMouse [Kohara et al., 2002]. However, little is known about the mechanism of in vivo mutagenesis by DNP.

To evaluate the mutagenicity of 1,6-DNP under exposure conditions appropriate for an air pollutant, the compound was administered intratracheally to *gpt*-delta mice. Treatment with 0–0.05 mg of this compound led to a linear increase in mutant and mutation frequency (Fig. 1), as shown previously with 0–2 mg B[*a*]P [Hashimoto et al., 2005]. The in vivo mutagenic potency (induced mutant frequency per amount of compound administered) for 1,6-DNP was 32×10^{-5} per mg, which was 13 times higher than that of B[*a*]P (2.4×10^{-5} per mg) [Hashimoto et al., 2005], indicating that 1,6-DNP was a

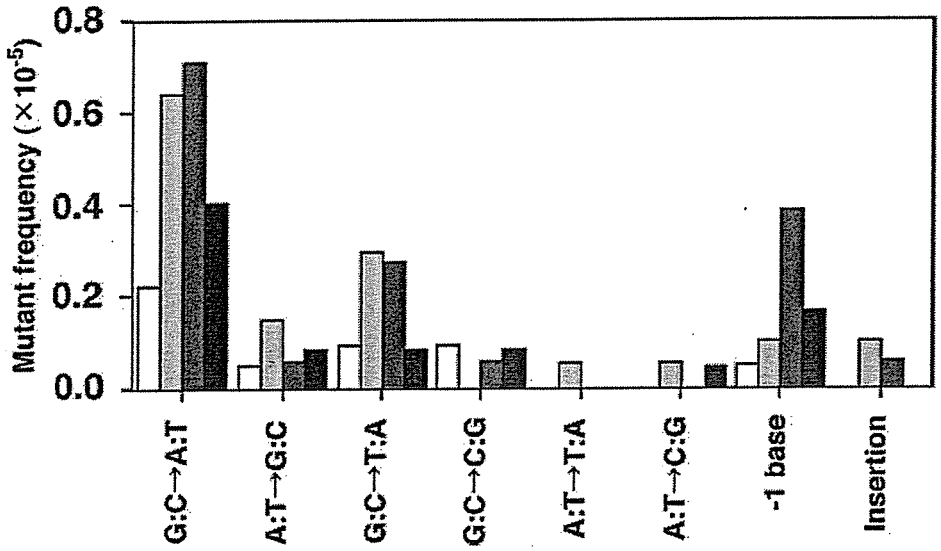

Fig. 2. Comparison of 1,6-DNP-induced and control mutation spectra in *gpt*-delta mice. White bar, control; light gray bar, 0.025 mg; dark gray bar, 0.05 mg; black bar, 0.1 mg. The analysis shown for control mutations is based on data combined from control animals in this study plus control animals from a previous study [Hashimoto et al., 2005].

more potent mutagen for the lung than B[*a*]P. However, the frequency was decreased at the highest dose (0.1 mg 1,6-DNP) to a lower level than that observed with 0.05 mg 1,6-DNP. We do not have any direct evidence to explain the decline in mutant frequency at high doses of 1,6-DNP in mice. Haugen et al. [1986] reported that unscheduled DNA synthesis, an index of excision repair in Clara cells and alveolar type-II cells, increased dose-dependently at low concentrations of 1,6-DNP, but decreased at high doses. This observation suggests that DNA adduct formation with 1,6-DNP is suppressed at high doses. Also, the amount of DNA adducts in 1,6-DNP-instilled rat lungs increased dose-dependently at low doses, but reached saturation at high doses [Smith et al., 1995]. The level of the 1,6-DNP-DNA adduct in lungs may be low at a dose of 0.1 mg 1,6-DNP, resulting in the lower mutant frequency. Finally it cannot be ruled out that cell proliferation in mice treated with 0.1 mg 1,6-DNP may not have been enough to fix the mutations because of the cytotoxicity of 1,6-DNP at high doses.

Our results indicate that G:C→A:T transitions, G:C→T:A transversions, and 1-base deletions are the major mutations induced by 1,6-DNP in the lung. On the other hand, Kohara et al. [2002] demonstrated that following the administration of DNP mixtures, the incidence of G:C→T:A transversions (43%) was higher than that of G:C→A:T transitions (22%) in the colon. Thus, the mutation spectrum of 1,6-DNP in the lung was different from the spectrum induced by the mixture of 1,3-, 1,6-, and 1,8-DNP in the colon. The metabolic reduction of 1,3-DNP and 1-nitropyrene was reported to be less extensive than that of 1,6- or 1,8-DNP, suggesting that the reduction pathways are distinct between these nitro-PAHs [Djuric et al., 1986]. Reduction as well as *O*-acetylation are important in determining the extent of DNA binding by 1,6- and 1,8-DNP in vivo [IPCS, 2003]. 1,6- and 1,8-DNP form *N*-(deoxyguanosin-8-yl)-1-amino-6-nitropyrene (dG-C8-1-amino-6-NP) and *N*-(deoxyguanosin-8-yl)-1-amino-8-nitropyrene (dG-C8-1-amino-8-NP) adducts, respectively [Smith et al., 1995; IPCS, 2003], while the adducts of 1,3-DNP have not been determined. We propose that differences in DNA adduct formation contribute to the variations in mutant spectra between 1,6-DNP and the 1,3-, 1,6-, and 1,8-DNP mixture.

Smith et al. [1997] reported that 1,6-DNP-induced lung tumors contain mutated K-*ras*. Among 20 specimens, 5 mutations in K-*ras* codon 12 (4 GGT to TGT transversions and 1 GGT to GAT), and 9 mutations in *p*53 exons 5–8 (8 substitutions at G:C base pairs and 1 deletion) were identified. These substitutions are consistent with the formation of dG adducts by 1,6-DNP. In our experiments, 1,6-DNP mainly induced substitutions in G:C pairs (61/77 = 79%), similar to the K-*ras* and *p*53 mutations in lung tumors.

Interestingly, we showed in an earlier report that the predominant mutations in the lungs of Big Blue rats exposed to 6 mg/m^3 DE for 1 month were G:C→A:T and A:T→G:C transitions [Sato et al., 2000]. The major mutations identified in the lungs of *gpt*-delta mice following exposure to 3 mg/m^3 DE for 3 months were G:C→A:T transitions (unpublished results, Hashimoto

TABLE III. DNA Sequence Analysis of *gpt* Mutation Obtained From the Lung of Control and 1,6-DNP-Treated *gpt*-delta Mice

Type of mutation in the *gpt* gene	Nucleotide	Sequence change	Site	Amino acid change	Number		Number		
					Control all	1,6-DNP all	0.025 mg of 1,6-DNP	0.05 mg of 1,6-DNP	0.1 mg of 1,6-DNP
Base substitution									
Transition									
G:C→A:T	26	tGg→tAg		Trp→Stop		1		1	
	64	Cga→Tga	CpG	Arg→Stop	1	5[a]	1	2[b]	2[b]
	92	gGc→gAc		Gly→Asp		1		1	
	110	cGt→cAt	CpG	Arg→His	1	12[c]	6	3[b]	3
	115	Ggt→Agt	CpG	Gly→Ser		4[c]	2[b]	1	1
	116	gGt→gAt		Gly→Asp		4[c]	1	2[b]	1
	128	gGt→gAt		Gly→Asp	1				
	401	tGg→tAg		Trp→Stop	1	1			1
	402	tgG→tgA		Trp→Stop		1			1
	406	Gaa→Aaa		Glu→Lys		2[b]		2[b]	
	417	tgG→tgA		Trp→Stop	1				
	418	Gat→Aat		Asp→Asn	2[b]	5[c]	3[b]	1	1
A:T→G:C	56	cTc→cCc		Leu→Pro		1			1
	149	cTg→cCg		Leu→Pro		1	1		
	275	gAt→gGt		Asp→Gly		2	2		
	419	gAt→gGt		Asp→Gly		2[b]		1	1
Transversion									
G:C→T:A	59	gCa→gAa		Ala→Glu		1			1
	115	Ggt→Tgt	CpG	Gly→Cys		1		1	
	140	gCg→gAg	CpG	Ala→Glu		1		1	
	244	Gaa→Taa	CpG	Glu→Stop	1				
	262	Gat→Tat		Asp→Tyr		2[b]	2[b]		
	287	aCt→aAt		Thr→Asn		3	3		
	402	tgG→tgT		Trp→Cys		1		1	
	406	Gaa→Taa		Glu→Stop		2[b]	1	1	
	413	cCg→cAg	CpG	Pro→Gln		1			1
	418	Gat→Tat		Asp→Tyr		1		1	
G:C→C:G	131	gCg→gGg	CpG	Ala→Gly		1		1	
	206	cGc→cCc	CpG	Arg→Pro		1			1
	413	cCg→cGg	CpG	Pro→Arg		1			1
A:T→T:A	10	Aaa→Taa		Lys→Stop		1	1		
A:T→C:G	106	Agc→Cgc		Ser→Arg		1			1
	254	aTc→aGc		Ile→Ser		1	1		
Deletion									
1-base	8–12	gAAAAAt→gAAAAt				1		1	
	32	aTg→ag				1		1	
	97	tAt→tt				1			1
	115–116	cGGt→cGt				1		1	
	126–128	cGGGt→cGGt				1		1	
	170–171	aCCg→aCg				1	1		
	237	gCg→gg				1			1
	278–279	aCCg→aCg				1			1
	315–318	cAAAAg→cAAAg				1	1		
	358–359	tCCg→tCg				2		2	
	416–418	tGGGa→tGGa			1	1		1	
	423–425	tGGGc→tGGc				1			1
Insertion									
	291	cg→cAg				2	2		
	255	cg→cGTTATTGATGACCTg				1		1	

[a]Mutation found in five different mice.
[b]Mutation found in two different mice.
[c]Mutation found in four different mice.

et al.). As observed in DE-exposed lungs, G:C→A:T transition was the major base substitution (47%, 36 out of 77 mutants) induced by 1,6-DNP (Fig. 2), while G:C→T:A transversions were the predominant base substitution in B[*a*]P-instilled lungs of *gpt*-delta mice [Hashimoto et al., 2005]. Our results provide useful information on the in vivo mutations induced by 1,6-DNP in the lung.

ACKNOWLEDGMENTS

The authors thank Dr. Hiroaki Shiraishi, Dr. Michi Matsumoto, and Dr. Wakae Maruyama for support and advice.

REFERENCES

Adams WT, Skopek TR. 1987. Statistical test for the comparison of samples from mutational spectra. J Mol Biol 194:391–396.

Brightwell J, Fouillet X, Cassano-Zoppi AL, Gatz R, Duchosal F. 1986. Neoplastic and functional changes in rodents after chronic inhalation of engine exhaust emissions. Dev Toxicol Environ Sci 13: 471–485.

Cariello NF, Piegorsch WW, Adams WT, Skopek TR. 1994. Computer program for the analysis of mutational spectra: Application to *p53* mutations. Carcinogenesis 15:2281–2285.

Delclos KB, Walker RP, Dooley KL, Fu PP, Kadlubar FF. 1987. Carcinogen-DNA adduct formation in the lungs and livers of preweanling CD-1 male mice following administration of [^{3}H]-6-nitrochrysene, [^{3}H]-6-aminochrysene, and [^{3}H]-1,6-dinitropyrene. Cancer Res 47:6272–6277.

Djuric Z, Potter DW, Heflich RH, Beland FA. 1986. Aerobic and anaerobic reduction of nitrated pyrenes in vitro. Chem Biol Interact 59:309–324.

Harris JE. 1983. Diesel emission and lung cancer. Risk Anal 3:83–100.

Hashimoto AH, Amanuma K, Hiyoshi K, Takano H, Masumura K, Nohmi T, Aoki Y. 2005. In vivo mutagenesis induced by benzo[*a*]pyrene instilled into the lung of *gpt* delta transgenic mice. Environ Mol Mutagen 45:365–373.

Haugen A, Aune T, Deilhaug T. 1986. Nitropyrene-induced DNA repair in Clara cells and alveolar type-II cells isolated from rabbit lung. Mutat Res 175:259–262.

IPCS (International Programme on Chemical Safety). 2003. Selected nitro- and nitro-oxy-polycyclic aromatic hydrocarbons.Environmental health criteria 229. Geneva:World Health Organization. pp 161–164.

Iwagawa M, Maeda T, Izumi K, Otsuka H, Nishifuji K, Ohnishi Y, Aoki S. 1989. Comparative dose-response study on the pulmonary carcinogenicity of 1,6-dinitropyrene and benzo[*a*]pyrene in F344 rats. Carcinogenesis 10:1285–1290.

Jeffrey AM, Santella RM, Wong D, Hsieh LL, Heisig V, Doskocil G, Ghayourmanesh S. 1990. Metabolic activation of nitropyrenes and diesel particulate extracts. Res Rep Health Eff Inst 34:1–30.

Kohara A, Suzuki T, Honma M, Oomori T, Ohwada T, Hayashi M. 2002. Dinitropyrenes induce gene mutations in multiple organs of the lambda/*lacZ* transgenic mouse (Muta Mouse). Mutat Res 515:73–83.

Masumura K, Matsui M, Katoh M, Horiya N, Ueda O, Tanabe H, Yamada M, Suzuki H, Sofuni T, Nohmi T. 1999. Spectra of *gpt* mutations in ethylnitrosourea-treated and untreated transgenic mice. Environ Mol Mutagen 34:1–8.

Masumura K, Matsui K, Yamada M, Horiguchi M, Ishida K, Watanabe M, Wakabayashi K, Nohmi T. 2000. Characterization of mutations induced by 2-amino-1-methyl-6-phenylimidazo[4,5-*b*]pyridine in the colon of *gpt* delta transgenic mouse: Novel G:C deletions beside runs of identical bases. Carcinogenesis 21:2049–2056.

Masumura K, Totsuka Y, Wakabayashi K, Nohmi T. 2003. Potent genotoxicity of aminophenylnorharman, formed from non-mutagenic norharman and aniline, in the liver of *gpt* delta transgenic mouse. Carcinogenesis 24:1985–1993.

Mermelstein R, Kiriazides DK, Butler M, McCoy EC, Rosenkranz HS. 1981. The extraordinary mutagenicity of nitropyrenes in bacteria. Mutat Res 89:187–196.

Muranaka M, Suzuki S, Koizumi K, Takafuji S, Miyamoto T, Ikemori R, Tokiwa H. 1986. Adjuvant activity of diesel-exhaust particulates for the production of IgE antibody in mice. J Allergy Clin Immunol 77:616–623.

Nakagawa R, Kitamori S, Horikawa K, Nakashima K, Tokiwa H. 1983. Identification of dinitropyrenes in diesel-exhaust particles. Their probable presence as the major mutagens. Mutat Res 124:201–211.

Nohmi T, Katoh M, Suzuki H, Matsui M, Yamada M, Watanabe M, Suzuki M, Horiya N, Ueda O, Shibuya T, Ikeda H, Sofuni T. 1996. A new transgenic mouse mutagenesis test system using Spi$^-$ and 6-thioguanine selections. Environ Mol Mutagen 28:465–470.

Nohmi T, Suzuki T, Masumura K. 2000. Recent advances in the protocols of transgenic mouse mutation assays. Mutat Res 455:191–215.

Rosenkranz HS, Mermelstein R. 1983. Mutagenicity and genotoxicity of nitroarenes. All nitro-containing chemicals were not created equal. Mutat Res 114:217–267.

Salmeen IT, Pero AM, Zator R, Schuetzle D, Riley TL. 1984. Ames assay chromatograms and the identification of mutagens in diesel particle extracts. Environ Sci Technol 18:375–382.

Sato H, Sone H, Sagai M, Suzuki KT, Aoki Y. 2000. Increase in mutation frequency in lung of Big Blue rat by exposure to diesel exhaust. Carcinogenesis 21:653–661.

Smith BA, Fullerton NF, Heflich RH, Beland FA. 1995. DNA adduct formation and T-lymphocyte mutation induction in F344 rats implanted with tumorigenic doses of 1,6-dinitropyrene. Cancer Res 55:2316–2324.

Smith BA, Manjanatha MG, Pogribny IP, Mittelstaedt RA, Chen T, Fullerton NF, Beland FA, Heflich RH. 1997. Analysis of mutations in the K-*ras* and *p53* genes of lung tumors and in the *hprt* gene of 6-thioguanine-resistant T-lymphocytes from rats treated with 1,6-dinitropyrene. Mutat Res 379:61–68.

Sugimura T, Takayama S. 1983. Biological actions of nitroarenes in short-term tests on *Salmonella*, cultured mammalian cells and cultured human tracheal tissues: Possible basis for regulatory control. Environ Health Perspect 47:171–176.

Suzuki T, Itoh S, Nakajima M, Hachiya N, Hara T. 1999. Target organ and time-course in the mutagenicity of five carcinogens in Muta-Mouse: A summary report of the second collaborative study of the transgenic mouse mutation assay by JEMS/MMS. Mutat Res 444:259–268.

Takano H, Yanagisawa R, Ichinose T, Sadakane K, Inoue K, Yoshida S, Takeda K, Yoshino S, Yoshikawa T, Morita M. 2002. Lung expression of cytochrome P450 1A1 as a possible biomarker of exposure to diesel exhaust particles. Arch Toxicol 76:146–151.

Takayama S, Ishikawa T, Nakajima H, Sato S. 1985. Lung carcinoma induction in Syrian golden hamsters by intratracheal instillation of 1,6-dinitropyrene. Jpn J Cancer Res 76:457–461.

Thybaud V, Dean S, Nohmi T, de Boer J, Douglas GR, Glickman BW, Gorelick NJ, Heddle JA, Heflich RH, Lambert I, Martus HJ, Mirsalis JC, Suzuki T, Yajima N. 2003. In vivo transgenic mutation assays. Mutat Res 540:141–151.

Tokiwa H, Otofuji T, Horikawa K, Kitamori S, Otsuka H, Manabe Y, Kinouchi T, Ohnishi Y. 1984. 1,6-Dinitropyrene: Mutagenicity in *Salmonella* and carcinogenicity in BALB/c mice. J Natl Cancer Inst 73:1359–1363.

Available online at www.sciencedirect.com
ScienceDirect
Mutation Research 609 (2006) 102–115
Genetic Toxicology and Environmental Mutagenesis
www.elsevier.com/locate/gentox
Community address: www.elsevier.com/locate/mutres

A newly established GDL1 cell line from *gpt* delta mice well reflects the in vivo mutation spectra induced by mitomycin C

Akira Takeiri [a,*], Masayuki Mishima [a], Kenji Tanaka [a], Akifumi Shioda [a], Asako Harada [a], Kazuto Watanabe [a], Ken-Ichi Masumura [b], Takehiko Nohmi [b]

[a] *Fuji Gotemba Research Laboratories, Chugai Pharmaceutical Co. Ltd., 1-135 Komakado, Gotemba, Shizuoka 412-8513, Japan*
[b] *Division of Genetics and Mutagenesis, National Institute of Health Sciences, 1-18-1 Kamiyoga, Setagaya, Tokyo 158-8501, Japan*

Received 8 May 2006; received in revised form 19 June 2006; accepted 30 June 2006
Available online 17 August 2006

Abstract

In order to create a novel in vitro test system for detection of large deletions and point mutations, we developed an immortalized cell line. A SV40 large T antigen expression unit was introduced into fibroblasts derived from *gpt* delta mouse lung tissue and a selected clone was established as the *gpt* delta L1 (GDL1) cell line. The novel GDL1 cells were examined for mutant frequencies (MFs) and for molecular characterization of mutations induced by mitomycin C (MMC). The GDL1 cells were treated with MMC at doses of 0.025, 0.05, and 0.1 μg/mL for 24 h and mutations were detected by Spi$^-$ and 6-thioguanine (6-TG) selections. The MFs of the MMC-treated cells increased up to 3.4-fold with Spi$^-$ selection and 3.5-fold with 6-TG selection compared to MFs of untreated cells. In the Spi$^-$ mutants, the number of large (up to 76 kilo base pair (kbp)) deletion mutations increased. A majority of the large deletion mutations had 1–4 base pairs (bp) of microhomology in the deletion junctions. A number of the rearranged deletion mutations were accompanied with deletions and insertions of up to 1.1 kbp. In the *gpt* mutants obtained from 6-TG selection, single base substitutions of G:C to T:A, tandem base substitutions occurring at the 5′-GG-3′ or 5′-CG-3′ sequence, and deletion mutations larger than 2 bp were increased. We compared the spectrum of MMC-induced mutations observed in vitro to that of in vivo using *gpt* delta mice, which we reported previously. Although a slight difference was observed in MMC-induced mutation spectra between in vitro and in vivo, the mutations detected in vitro included all of the types of mutations observed in vivo. The present study demonstrates that the newly established GDL1 cell line is a useful tool to detect and analyze various mutations including large deletions in mammalian cells.

Keywords: Mitomycin C; Cell line; *gpt* delta mice

1. Introduction

Point mutations and deletion mutations are major genotoxic events induced by chemicals and ionizing radiation. In particular, deletion mutations constitute an important class of mutations that may result in a variety of human diseases including cancer [1]. Development of various in vivo test systems suitable for detection and analysis of point mutations have provided a better understanding of molecular properties of chemical mutagenesis [2,3]. However, fewer methodologies are available to analyze deletion mutations compared with

* Corresponding author. Tel.: +81 550 87 6376; fax: +81 550 87 6383.
E-mail address: takeiriakr@chugai-pharm.co.jp (A. Takeiri).

1383-5718/$ – see front matter © 2006 Elsevier B.V. All rights reserved.
doi:10.1016/j.mrgentox.2006.06.026

point mutations. Recently, successful and convenient approaches for the analysis of deletion mutations using transgenic (TG) animal models have been constructed [4,5]. The *lacZ* plasmid-based TG mouse assay detects deletion mutations induced by X-ray and cisplatin [5,6]. The *gpt* delta mice efficiently detects deletion mutations induced by various mutagens, e.g., mitomycin C (MMC) [7,8], heavy-ion, X-ray [9], gamma-ray [9,10], and ultraviolet B [11,12]. In the *gpt* delta mice, approximately 80 copies of the lambda EG10 shuttle vector DNA carrying the *red/gam* genes of lambda phage and the *gpt* gene of *Escherichia coli* are integrated into this TG mouse on chromosome 17 of the C57BL/6J background [2,4]. Deletion mutations in the *red/gam* genes and point mutations in the *gpt* gene can be individually identified by Spi^- (sensitive to P2 interference) selection and 6-thioguanine (6-TG) selection, respectively [2].

MMC is a natural cytotoxic and genotoxic agent used in clinical anticancer chemotherapy [13]. The mode of action of this agent in mutagenicity is intriguing and well investigated. MMC alkylates DNA in several different ways [14]. It binds to the N^2 position of guanine in DNA and forms monoalkylation products. Furthermore, after the carbamate at C-10″ is lost, it will give rise to another active site capable of alkylating the second guanine within the DNA. Alkylation of two guanine bases on the same DNA strand results in the formation of intrastrand cross-links within the 5′-GG-3′ sequence, and the alkylation of guanine bases on opposite DNA strands leads to the formation of interstrand cross-links within the 5′-CG-3′ sequence [15–19]. Interaction of MMC and DNA strands causes the production of characteristic mutations. In our previous in vivo study, MMC-induced tandem base substitutions and deletion mutations up to about 8 kilo base pair (kbp) in size [8].

Since it is often advantageous to use in vitro test systems in mechanistic investigations, we newly established the GDL1 cell line harboring the same reporter gene system as *gpt* delta mice. The cells were established from lung fibroblasts of the *gpt* delta mice with a functional reduction of p53 protein by intracellular expression of the Simian virus 40 large T antigen (SV40 T antigen). GDL1 was exposed to MMC to characterize the induced mutations. Comparing the results from GDL1 cells with those previously reported in vivo, there was little difference in mutation spectra and all of the types of mutations in vivo were involved in the events detected with GDL1 cells. The GDL1 cell is a novel tool available for molecular analysis of deletion mutations. Furthermore, we here discuss the contribution of the dysfunction of p53 by the SV40 T antigen to the differences between the MMC-induced mutations in the GDL1 cells and in the *gpt* delta mice.

2. Materials and methods

2.1. Collection of the fibroblasts

Lung tissues were obtained from 21-week-old female *gpt* delta mice maintained in our laboratory. The tissues were minced in Eagle's minimum essential medium (MEM, Sigma–Aldrich, St. Louis, MO, USA) and trypsinized in MEM including 0.1% (w/v) trypsin, 0.01% (w/v) EDTA for 1 h at 37 °C. After centrifugation, the down pellet containing fibroblast cells was suspended in Dulbecco's modified Eagle's medium (DMEM, Sigma–Aldrich, St. Louis, MO, USA) including 10% (v/v) fetal bovine serum (FBS, Invitrogen, Carlsbad, CA, USA). The cells were cultured in 75-cm^2 culture flasks (BD Biosciences, Franklin Lakes, NJ, USA) in an atmosphere of 5% CO_2 at 37 °C.

2.2. Establishment of the cell line

A plasmid encoding the complete sequence for the SV40 T antigen was obtained from the Health Science Research Resources Bank (Osaka, Japan): pMTIOD, registration no. VG026 [20]. The complete sequence of the T antigen gene was excised from pMTIOD and inserted into an expression vector at the downstream of the elongation factor 1 alpha promoter, resulting in pCOSV1. The constructed vector was introduced into the fibroblasts using a lipofection reagent, FuGENE6 (Roche Diagnostics, Tokyo, Japan). The transfectants were selected by culture in DMEM containing 100 μg/mL of G-418 for 1 week. The cells were cloned and, after approximately 60 passages in DMEM supplemented with 10% (v/v) FBS in an atmosphere of 5% CO_2 at 37 °C, we selected a stably growing single clone (clone #2) to establish the GDL1 cell.

2.3. Measurement of chromosome number and immunostaining

A single cloned GDL1 cell stock frozen in liquid nitrogen was thawed and maintained in DMEM supplemented with 10% (v/v) FBS in an atmosphere of 5% CO_2 at 37 °C. For measurement of chromosome number, the cells were treated with 0.1 μg/mL colcemid (Wako Pure Chemical Industries, Osaka, Japan) for 2 h. The trypsinized cells using PBS including 0.1% (w/v) trypsin, 0.01% (w/v) EDTA were suspended in 75 mM KCl hypotonic solution and fixed with acetic acid and methanol (1:3) mixture. The cell suspensions were dropped on glass slides and dried. The metaphase spreads of the cells were stained with Giemsa and each chromosome of 100 metaphases was scored. The cells cultured in a 24-well culture plate (BD Biosciences, Franklin Lakes, NJ, USA) were fixed by 99.5% methanol and then examined for SV40 T antigen expression by immunofluorescent assay. The cells were stained with anti-

SV40 large T monoclonal antibody, SV40T-Ag (Ab-2) (EMD Biosciences, San Diego, CA, USA), and FITC conjugated anti-mouse immunoglobulin polyclonal antibody (Dako Cytomation, Carpinteria, CA, USA).

2.4. Cytotoxicity

GDL1 cells were seeded in 12-multiwell culture plate (Corning, Corning, NY, USA) at a density of 4×10^4 cells/mL in each well. One day after the seeding, the cells were treated with mitomycin C (MMC, CAS no. 50-07-7, Kyowa Hakko Kogyo, Tokyo, Japan) at doses of 0.025, 0.05, and 0.1 μg/mL for 24 h. The solutions of chemicals were freshly prepared at 100-fold of final concentration in saline. The cells were trypsinized and resuspended in DMEM supplemented with 10% (v/v) FBS. The number of cells was counted using automated hematology analyzer KX-21 (Sysmex, Kobe, Japan).

2.5. Treatment with MMC and preparation of lambda EG10 phage

GDL1 cells were subcultured and divided into flasks for chemical treatment at 1×10^5 cells/5 mL medium per 25-cm^2 culture flask 2 days before the treatment. Three culture flasks were prepared for each dose of MMC and untreated control. The cells were exposed to MMC at doses of 0.025, 0.05, or 0.1 μg/mL for 24 h, washed, and cultured for an additional 6 days. The additional 6 days is considered sufficient for fixation of mutations [21]. During the 6-day culture, the cells were subcultured two times; the culture volume was increased to 10 mL and transferred to 75-cm^2 culture flasks. DNA samples of the cells were prepared using a RecoverEase DNA isolation kit (Stratagene, La Jolla, CA, USA). The lambda EG10 phages were rescued from the DNA by in vitro packaging reaction using Transpack packaging extract (Stratagene, La Jolla, CA, USA) according to the manufacturer's instruction.

2.6. Measurement of mutant frequency (MF) and sequence analysis

The Spi$^-$ mutation assay was performed as described previously [2,10,12]. The rescued phages were infected to *E. coli* XL1-Blue MRA (P2) (Stratagene, La Jolla, CA, USA). The infected host cells were poured onto lambda-trypticase agar plates and incubated at 37 °C to detect mutant phage plaque. The rescued phages were diluted and infected to *E. coli* XL1-Blue MRA (Stratagene, La Jolla, CA, USA) to determine total number of phage plaques. The Spi$^-$ MF was calculated as previously reported [2,10,12]. The entire sequence of lambda EG10 phage and the detail method of Spi$^-$ selection and 6-TG selection is available at: http://www.dgm2alpha.nihs.go.jp/dgm2/.

The *gpt* mutagenesis assay was performed according to previous method [2,11]. Briefly, the lambda EG10 phages were converted to plasmids by the infection to *E. coli* YG6020 which was expressing Cre recombinase. The infected bacteria were poured onto agar plates containing chloramphenicol (Cm) and 6-TG. The plates were incubated at 37 °C for the selection of colonies harboring plasmids carrying the mutated *gpt* gene. The infected host bacteria were diluted and poured on the plates containing Cm alone to determine the total number of rescued plasmids. The *gpt* MF was calculated as previously reported [2,11].

In the cells treated with 0.1 μg/mL MMC or untreated, the Spi$^-$ mutants and *gpt* mutants obtained from Spi$^-$ selection and 6-TG selection, respectively, were used for sequence analysis as previously described [2,8,10–12]. The sequences of the *gam* gene or DNA sequences surrounding the deletion junction were analyzed in 43 Spi$^-$ mutants from untreated cells and 45 mutants from MMC-treated cells. Forty-five *gpt* mutants each from untreated and MMC-treated cells were analyzed. In Spi$^-$ mutants and *gpt* mutants, the mutations analyzed were classified by the types of mutation. The ratio of each type of mutation to total mutation was multiplied by total MF for calculation of specific MF. The specific MFs of the MMC-treated cells were statistically compared to those of the control cells using Fisher's exact test according to the method of Carr and Gorelick [22].

3. Results

3.1. Induction of Spi$^-$ and gpt mutations by MMC in GDL1 cells

We established the GDL1 cell line from fibroblasts of the lung of *gpt* delta TG mice by introduction of plasmid pCOSV1 expressing SV40 T antigen. The doubling time of the cell line was approximately 12 h (data not shown), and the cells were polyploid with a modal chromosome number of 74 ($2N=40$ in mice) (Fig. 1). SV40 T antigen was expressed and localized in the nucleus (data not shown). To characterize the GDL1 cell line as a tester for genotoxicity assays, we examined the Spi$^-$ and *gpt* mutations induced by MMC at the molecular

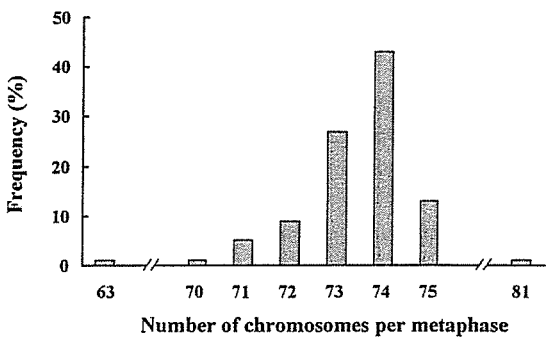

Fig. 1. Chromosome frequency distribution in GDL1 cells. The number of chromosomes in a spread of 100 metaphase cells was calculated. The modal chromosome number was 74 ($2N=40$ in mice).

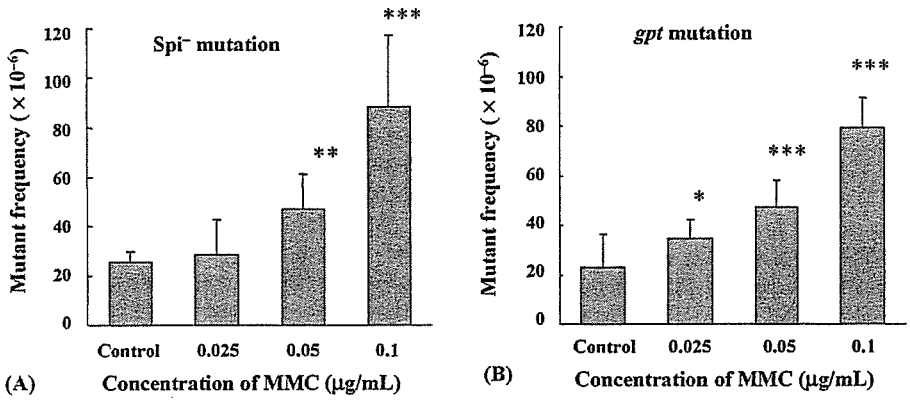

Fig. 2. Mutant frequencies in MMC-treated GDL1 cells. (A) Spi⁻ mutant frequencies; (B) *gpt* mutant frequencies. Cells were treated with MMC at the doses of 0.025, 0.05, and 0.1 μg/mL for 24 h. After a 6-day culture, the cells were harvested. As the control, untreated cells were collected after a 6-day cell culture. Spi⁻ mutant frequency in Spi⁻ selection and *gpt* mutant frequency in 6-TG selection were determined. *P* values calculated by Fisher's exact test were $P<0.05$ (*), $P<0.001$ (**), and $P<0.0001$ (***). Bars represent mean and standard deviations of data obtained from three independent cell culture flasks.

level. In the MMC-treated group, Spi⁻ MFs at concentrations of 0.025, 0.05, and 0.1 μg/mL were 28.4×10^{-6}, 47.0×10^{-6}, and 88.0×10^{-6}, respectively (Fig. 2A). MFs increased in a dose-dependent manner up to 3.4 times higher than the control group, i.e., 25.6×10^{-6}. On the other hand, *gpt* MFs at concentrations of 0.025, 0.05, and 0.1 μg/mL were 34.8×10^{-6}, 47.0×10^{-6}, and 78.9×10^{-6}, respectively (Fig. 2B). The *gpt* MFs increased in a dose-dependent manner up to 3.5-fold compared with the control group, i.e., 22.7×10^{-6}. The numbers of cells treated with MMC for 24 h were 73, 53, and 40% of untreated cells in 0.025, 0.05, and 0.1 μg/mL of MMC, respectively.

3.2. Molecular nature of Spi⁻ mutations induced by MMC

To characterize the molecular nature of Spi⁻ mutations induced by MMC, we sequenced 43 and 45 Spi⁻ mutants from untreated cells and cells treated with MMC (0.1 μg/mL), respectively, and categorized them into five classes (Table 1). The specific MF for each class and subclass was determined by multiplying the percentage of each class of mutants and the total MF, and the calculated values were compared between untreated and treated groups.

Large deletions more than 1 kbp in deletion size were classified as class I. They were subclassified into classes I-A and I-B depending on the existence of homologous sequences at the junctions. The specific MF class I-A, i.e., large deletion with short homology (microhomology) at the junction, was enhanced more than four-fold by treatments with MMC (17.6×10^{-6} versus 4.2×10^{-6}, Table 1). The deletion sizes of nine class I-A mutants from the MMC-treated group were from 3829 to 7178 base pair (bp) (Fig. 3). They were all unique in size and position of the deletions. In addition, three class I-B mutants, i.e., large deletions without short homologous sequence, were identified in the treated group. Two of them were simple deletion mutants with deletion sizes of 3345 and 5204 bp, but one mutant, sM2-3, had an insertion of 16 bp with a deletion size of 5676 bp (Fig. 3). In contrast, class I mutants of the untreated group were all class I-A and no class I-B mutants were identified. Five of seven class I-A mutants from untreated cells were completely the same in size and position of deletions (Fig. 3). Since they were independently identified in the mutants and derived from independent culture flasks, they might have been generated by hot spot mutations in untreated GDL1 cells. Alternatively, the mutation might have occurred prior to the subculture of the cells for untreated groups (clonally expanded mutants). The deletion sizes of the seven class I-A mutants were from 3308 to 6827 bp.

Midsized deletions with sizes of from 2 bp to 1 kbp were classified as class II. The specific MF for class II was enhanced more than six times by the treatments with MMC (7.8×10^{-6} versus 1.2×10^{-6}, Table 1). The deletion sizes of four mutants in the MMC-treated group were from 9 to 129 bp (Fig. 3). They were all unique in size and position of the deletions. Two of them were simple deletion mutants with deletion sizes of 9 and 129 bp, and the deleted regions were flanked by two short homologous sequences. Other two deletions had flush ends but had insertions of 9 and 8 bp in the junctions. The deleted sequences were enclosed by short repetitive sequences.

Table 1
Summary of Spi$^-$ mutations derived from the GDL1 cells

Type of mutation	Class of mutation	Control		MMC		*P* value[a]
		No. of mutants (%)	Specific MF[b] ($\times 10^{-6}$)	No. of mutants (%)	Specific MF[b] ($\times 10^{-6}$)	
Large deletion (>1 kbp)						
With microhomology	I-A	7 (16.3)	4.2	9 (20.0)	17.6	<0.01
Without microhomology	I-B	0 (0.0)	0.0	3 (6.7)	5.9	<0.05
Midsize deletion (2 bp to 1 kbp)	II	2 (4.7)	1.2	4 (8.9)	7.8	<0.05
Single base deletion						
At run sequence	III-A	29 (67.4)	17.3	17 (37.8)	33.2	0.06
At non-run sequence	III-B	2 (4.7)	1.2	0 (0.0)	0.0	1.00
Complex mutation	IV	0 (0.0)	0.0	5 (11.1)	9.8	<0.001
Miscellaneous mutation	V					
Transversion						
G:C → T:A		2 (4.7)	1.2	0 (0.0)	0.0	1.00
A:T → T:A		0 (0.0)	0.0	2 (4.4)	3.9	0.06
Tandem base substitution						
GG:CC → TA:AT		0 (0.0)	0.0	1 (2.2)	2.0	0.24
GG:CC → TT:AA		0 (0.0)	0.0	1 (2.2)	2.0	0.24
Other substitution		1 (2.3)	0.6	2 (4.4)	3.9	0.15
Unidentified		0 (0.0)	0.0	1 (2.2)	2.0	0.24
Total		43 (100)	25.6	45 (100)	88.0	<0.0001

[a] *P* values were determined using Fisher's exact test according to Carr and Gorelick [22].
[b] Specific MF was calculated by multiplying the total mutation frequency by the ratio of each type of mutation to the total mutation.

In the control group, two of the class II mutations were simple deletions with sizes of 13 and 206 bp.

Single base deletions occurring in the *gam* gene were classified as class III with subclasses of classes III-A and III-B. Single base deletion induced at a run sequence of identical bases, e.g., −1A deletion at 5′-AAAAAA-3′ of nucleotides 295–300 (Fig. 4), were classified as class III-A and single base deletions occurring at a non-run sequence were classified as class III-B. The specific MF of class III-A was enhanced about two times by the MMC treatments (33.2×10^{-6} versus 17.3×10^{-6}, Table 1). The class III-A was dominant over III-B in both MMC-treated and control groups.

Complex mutations were classified as class IV. Five mutants of this class were observed in the MMC-treated group, while no such mutants were observed in the control group. All five MMC-induced class IV mutations were deletions with complex rearrangements (Figs. 3 and 5). Mutant sM1-9, with a deleted region of approximately 5 kbp, had an inserted fragment larger than 1 kbp, which was homologous to the sequence in chromosome 16 of mouse from the DNA data base (http://www.ddbj.nig.ac.jp/). Since the lambda EG10 DNA is integrated in chromosome 17 of the *gpt* delta mouse, the mutation was due to inter-chromosomal translocation. In mutant sM2-6, a 7632 bp region including the *red/gam* genes was deleted, and three DNA fragments derived from the deleted region – fragment 1 (457 bp), fragment 2 (153 bp), and fragment 3 (1115 bp) – were incorrectly inserted again. In mutant sM2-12, a region of 3459 bp was deleted and a fragment of 403 bp, which was located at approximately 1.2 kbp from the deleted site, was inserted into the deletion site. In mutant sM2-14, the deletion size was approximately 5 kbp. A sequence existing approximately 6 kbp away from the deletion site was inserted into the deletion junction in the opposite direction. The accurate size of the inserted fragment was not determined. In mutant sM3-7, the deletion size determined by agarose-gel electrophoresis of the PCR product was approximately 5 kbp. A DNA fragment located approximately 18 kbp away from the deletion site was inserted into the deletion site. The size of the inserted fragment could not be determined accurately. Almost all of the deletion junctions observed in the complex rearrangements mentioned above had microhomology sequences (Fig. 3).

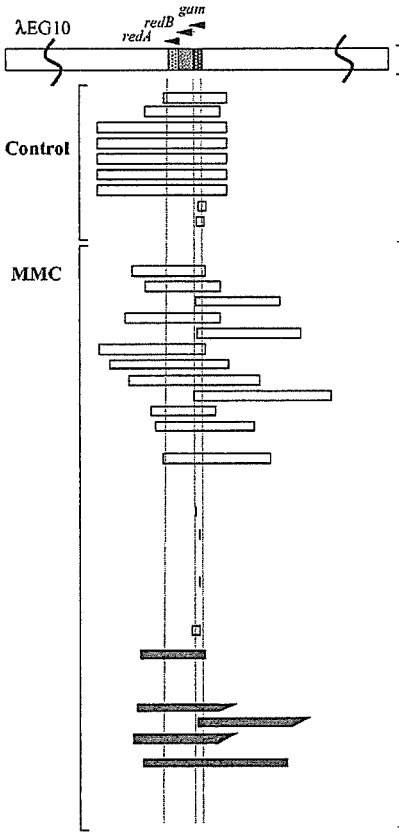

Treatment	Mutant code	Class	Mutation	Sequence of deletion junction
Control	sC3- 3	I-A	-3,308 bp deletion	TTCCTGGTGTTTCTT TCTTCTGTTGAGTTA
	sC2- 1	I-A	-3,979 bp deletion	TTATTGAAAAATAAA TAAACTGGAAAGCAA
	sC1- 8	I-A	-6,827 bp deletion	TTGTTTTACTGCGGG GATGAATCCGTCAGT
	sC1- 9	I-A	-6,827 bp deletion	TTGTTTTACTGCGGG GATGAATCCGTCAGT
	sC2- 7	I-A	-6,827 bp deletion	TTGTTTTTCTGCGGG GATGAATCCGTCAGT
	sC3- 9	I-A	-6,827 bp deletion	TTGTTTTACTGCGGG GATGAATCCGTCAGT
	sC3- 10	I-A	-6,827 bp deletion	TTGTTTTACTGCGGG GATGAATCCGTCAGT
	sC1- 2	II	-13 bp deletion	CGTCACTACCAGCAG AGAGAAAGAGGCAGA
	sC3- 11	II	-206 bp deletion	CTAATCAGCCCGGCA ACGGGGCCAGCAAAA
MMC 0.1 μg/mL	sM1- 7	I-A	-3,829 bp deletion	GATGTTTCGTGAAGC CGGTGGAAACGATAC
	sM1- 10	I-A	-3,979 bp deletion	TTATTGAAAAATAAA TAAACTGGAAAGCAA
	sM1- 12	I-A	-4,424 bp deletion	TGCAGGATATCGACC ACCATTGCTCACCAC
	sM3- 12	I-A	-4,996 bp deletion	CTACCAAACAATGCC GCCTTGAAACAGTTC
	sM3- 11	I-A	-5,454 bp deletion	ACGCGGCGCTCGATG GATGACGATGTTGAG
	sM2- 9	I-A	-5,618 bp deletion	CTAACCCCCTTTCCT CTTTACTGCCATATT
	sM2- 15	I-A	-6,230 bp deletion	TGCAGGAACCATGAT GATATCTTTATGTCG
	sM3- 15	I-A	-6,823 bp deletion	AGGAACAACTGCCGG GGAGAATGGAATGGA
	sM1- 15	I-A	-7,178 bp deletion	ATGATAACCATTGCG CGTGTCGGCATGGAT
	sM3- 13	I-B	-3,345 bp deletion	AAGGCTTTGGGGTGT ACGCCTGGTCGTTCA
	sM3- 1	I-B	-5,204 bp deletion	GGAGAGATCCCCTGGC GGAGCTACAGGCTCC
	sM2- 3	I-B	-5,676 bp deletion, +16 bp insertion	TTTTTACCGCCAGAT AGCCGCATCCCTTTC ^ AATGGTCTGCGCTTGA
	sM3- 4	II	-9 bp deletion	CATGGCAGAACACAT ATGGTTGAAACCATT
	sM2- 10	II	-13 bp deletion, +9 bp insertion	CACTACCAGCAGCTC ^ CTGAGCCTC AAGAGGCAGAACTGG
	sM3- 9	II	-36 bp deletion, +8 bp insertion	GTCTTGAGGCTCAGA ^ CGATCACT AGAAAGAGGCAGAAC
	sM2- 11	II	-129 bp deletion	AACACATCCGGTACA AACTGATCACCACTC
	sM2- 12	IV	-3,459 bp and -405 bp deletion +403 bp and +28 bp insertion	ATGGCTTGATCGCTA AAATGAAGTGGTCTG GCCACTTTTATTGGC TGGCCAGCAGAGGAA TGCGAAATGAAGTGG GAAAATGCTGAATTT
	sM3- 7	IV	approx. -5 kbp deletion, insertion	AGAATCCAGATGGAT ATCAATGTTGTGCAG
	sM2- 14	IV	approx. -5 kbp deletion, reverse-fragment insertion	AGCCCACAATGCCGC CATCGATCATTTGCA
	sM1- 9	IV	approx. -5 kbp deletion, inter-chromosomal translocation	TTTATTTCCACTTTT CAATATTACATAACA
	sM2- 6	IV	-7,632 bp deletion, +153 bp insertion and two reverse-fragments (+457 bp and +1,115 bp) insertion	CGCCAGCGACGCACG CGCTATTACGGGGTT TCCCTGCCGTTAGCG GCGTCCAGTACGTGG GCGGGAGAGCAGGCGG GCGGGTTGTGGACCT CGCAGGCATTACGTG TGTAATTCTTCTATT

Fig. 3. Deletion mutations classified as classes I-A, I-B, II, and IV recovered from MMC-treated and untreated cells. A partial genetic map of the lambda EG10 transgene, including the *gam* and the *redBA* target regions of Spi$^-$ selection is shown. Horizontal bars represent regions deleted in Spi$^-$ mutants. Open bars represent the deleted regions of classes I-A, I-B, and II mutants, which have no rearrangements. Closed bars show class IV deletions, which have rearrangements within the deleted regions. An angled end of a bar denotes that the deletion positions have not been precisely determined. Junctions are indicated as a space between the left and right sequences. Microhomology sequences in the junctions are underlined. One of two microhomologies in the junctions that are underlined is deleted when the two DNA fragments are joined. (^) The insertion of a sequence in the deletion junction. All the mutants were analyzed with mutant codes. The first letter in the mutant code, 's' stands for Spi$^-$ mutants. 'M' stands for MMC-treated group and 'C' for the untreated control group. The third number is the ID number for the independent culture flask. The last number is the mutant ID number. The sM2-3 represents the Spi$^-$ mutants ID #3 in the MMC-treated flask #2.

Miscellaneous mutations including base substitutions in the *gam* gene were classified as class V (Table 1). In the MMC-treated group, tandem base substitutions at 5′-GG-3′ were observed.

3.3. Molecular characteristics of gpt mutations induced by MMC

To analyze MMC-induced point mutations, 45 mutations observed in the MMC-treated cells and 46 mutations derived from untreated control cells were identified at the sequence level (Table 2). Specific MFs of single base substitutions of G:C to T:A (substitutions of G to T or substitutions of C to A in Fig. 6) was 6.7-fold higher in the MMC-treated group than in the untreated group (26.3×10^{-6} versus 3.9×10^{-6}, Table 2). In the MMC-treated group, 19 of 26 (73%) single base substitutions was observed in the 5′-CG-3′ or 5′-GG-3′ sequence, in which MMC monoadducts were preferentially induced (Fig. 6) [23,24]. In the control group, 18 of 34 (53%) single base substitutions occurred at the 5′-CG-3′ or 5′-GG-3′ sequence (Fig. 6).

For insertion mutations with an insertion size larger than 2 bp, specific MF was 3.5×10^{-6} in the MMC-treated group, while no such mutations were observed in the control group (Table 2). The two mutations induced by MMC treatment were both 9 bp insertions (Fig. 6). One had a sequence change of 5′-GCGcagaagGCG-3′ to 5′-GCGcagaaggcgcagaagGCG-3′ in nucleotide 229–230 in the *gpt* gene, and the other had 5′-TCCcgccaatcTCC-3′ to 5′-TCCgccaatctccgccaatcTCC-3′ in nucleotide 438–439 (the sequences underlined

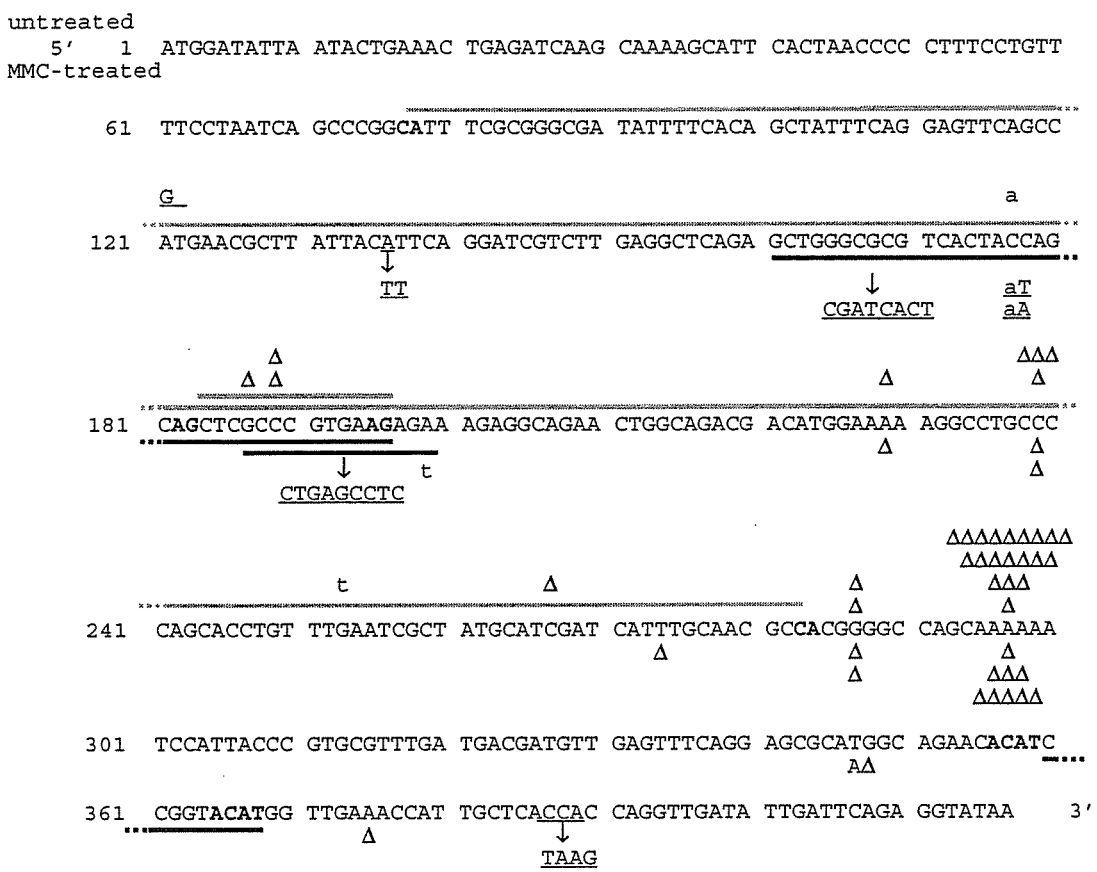

Fig. 4. Spi⁻ mutants of classes II, III-A, III-B, and V in the *gam* gene. The sequence from top to bottom represents the coding region of the *gam* gene. Mutations shown below the strands were detected in MMC-treated cells; those above the strands were observed in untreated cells. (Δ) Single base deletion. Sequence substitutions are underlined, the underlined sequences in the strands were substituted for the underlined sequence represented below the strands. Bars represent a deleted sequence in deletion mutations. The short homologous sequences associated with deletions are represented in bold. Two deletion mutations with sequence substitution in MMC-treated cells were substitutions of 5′-gctgggcgcgtcactaccagcagctcgcccgtgaag-3′ to 5′-cgatcact-3′ and 5′-gcccgtgaagaga-3′ to 5′-ctgagcctc-3′, and were classified as class II. The lowercase letters in the substituted sequences formed stop codon with adjoining two bases.

are altered sequences and the capital letters represent microhomology). In the former and latter mutants, 5′-cagaaggcg-3′ and 5′-cgccaatctc-3′, respectively, were repeated.

In deletion mutations larger than 2 bp, the specific MF in the MMC-treated group was 14 times higher than the untreated group (7.0×10^{-6} versus 0.5×10^{-6}, Table 2). In the MMC-treated group, four such deletions were identified (Fig. 6). They were an 8-bp deletion in 5′-CtcgcaagC-3′ of position 56–63, a 5-bp deletion in 5′-TaccgT-3′ of position 169–173, a 20-bp deletion in 5′-TCgcaaaaccggctggtcgTC-3′ of position 339–358, and a 329-bp deletion in 5′-CACTTcacatg· · ·aaagcgCACTT-3′ of position −3 to 326 in the *gpt* gene (not shown). All these deletions were enclosed by microhomology sequences. In the control group, one deletion with a size of 6 bp in 5′-GGCgaaGGC-3′ of position 241–246 was identified.

The specific MF of tandem base substitutions was 8.8×10^{-6} in the MMC-treated group, whereas no such mutations were observed in the untreated group. All five tandem base substitutions in the MMC-treated cells occurred in the 5′-GG-3′ or 5′-CG-3′ sequence, in which formation of MMC cross-links has been reported [15,16].

The specific MF of "others" was enhanced 14-fold by MMC treatments (7.0×10^{-6} versus 0.5×10^{-6}, Table 2). Four such MMC-induced mutations include a sequence substitution of 5′-TACCG-3′ to 5′-AACTA-3′ in position 122–126, a substitution 5′-CGG-3′ to 5′-AT-3′ in position 347–349, a −565-bp deletion accompanied by +1 bp insertion in position 11–575 (not shown) and a

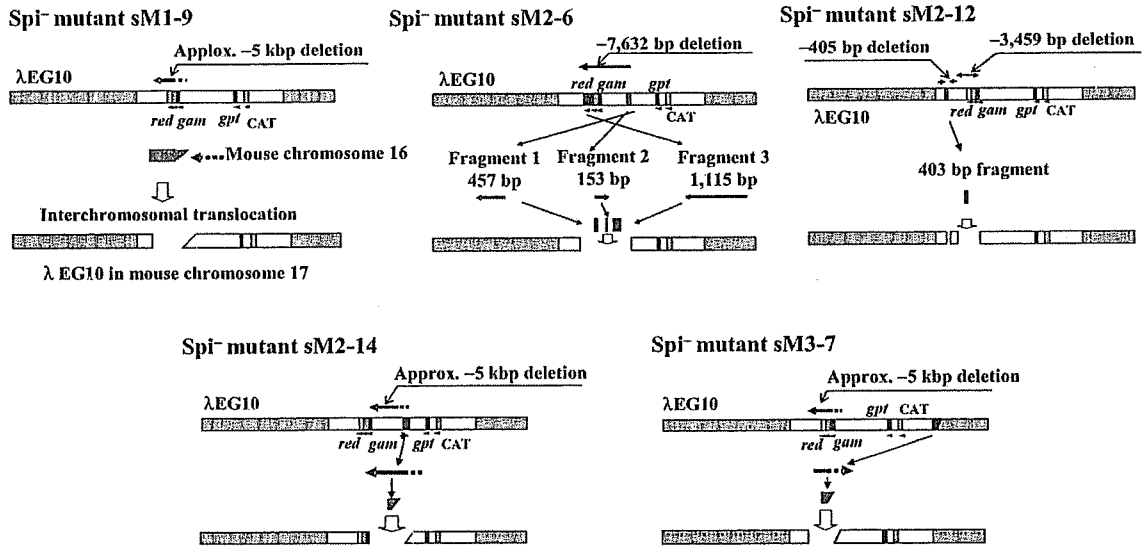

Fig. 5. Rearrangements induced in the Spi⁻ mutants derived from MMC-treated GDL1 cells. Complex deletions with insertions were observed in 5 Spi⁻ mutants. The upper bars in each mutant represent the lambda EG10 gene. The lower bars show mutants that have deletions and insertions resulting from MMC treatment. In the Spi⁻ mutant sM1-9, approximately 5 kbp were deleted. The inserted sequence was not found in the lambda EG10 gene but in chromosome 16 of the mouse genome. In Spi⁻ mutant sM2-6, 7632 bp including the *gam* gene sequence was deleted, and three DNA fragments within the deleted sequence, fragment 1 (457 bp), fragment 2 (153 bp), and fragment 3 (1115 bp), were inserted. The direction and order of the inserted fragments were different from that of the original sequence. In Spi⁻ mutant sM2-12, a fragment of 3459 bp including the *gam* gene was deleted and a fragment of 403 bp was inserted into the deletion site. In Spi⁻ mutant sM2-14, the deletion size was approximately 5 kbp. An inverted sequence existing approximately 6 kbp from the deletion site was inserted into the deletion junction. In Spi⁻ mutant sM3-7, the deletion size was approximately 5 kbp. A DNA fragment located approximately 18 kbp from the deletion site was inserted into the deletion site.

Table 2
Summary of *gpt* mutations derived from the GDL1 cells

Type of mutation	Control		MMC		*P* value[a]
	No. of mutants (%)	Specific MF[b] ($\times 10^{-6}$)	No. of mutants (%)	Specific MF[b] ($\times 10^{-6}$)	
Base substitution/single					
Transition					
G:C → A:T	13 (28.3)	6.4	7 (15.6)	12.3	0.18
A:T → G:C	3 (6.5)	1.5	2 (4.4)	3.5	0.31
Transversion					
G:C → T:A	8 (17.4)	3.9	15 (33.3)	26.3	<0.0001
G:C → C:G	1 (2.2)	0.5	1 (2.2)	1.8	0.40
A:T → T:A	4 (8.7)	2.0	0 (0.0)	0.0	0.58
A:T → C:G	5 (10.9)	2.5	1 (2.2)	1.8	1.00
Insertion					
+1A	2 (4.3)	1.0	0 (0.0)	0.0	1.00
+1T	3 (6.5)	1.5	2 (4.4)	3.5	0.31
>+2 bp	0 (0.0)	0.0	2 (4.4)	3.5	<0.05
Deletion					
−1A	1 (2.2)	0.5	0 (0.0)	0.0	1.00
−1G	2 (4.3)	1.0	0 (0.0)	0.0	1.00
−1C	2 (4.3)	1.0	2 (4.4)	3.5	0.22
>−2 bp	1 (2.2)	0.5	4 (8.9)	7.0	<0.05
Base substitution/tandem					
GG:CC → TC:AG	0 (0.0)	0.0	2 (4.4)	3.5	<0.05
GG:CC → TT:AA	0 (0.0)	0.0	2 (4.4)	3.5	<0.05
CG:GC → AA:TT	0 (0.0)	0.0	1 (2.2)	1.8	0.22
Others	1 (2.2)	0.5	4 (8.9)	7.0	<0.05
Total	46 (100)	22.7	45 (100)	78.9	<0.0001

[a] *P* values were determined using Fisher's exact test according to Carr and Gorelick [22].
[b] Specific MF was calculated by multiplying the total mutation frequency by the ratio of each type of mutation to the total mutation.

complex mutation, i.e., gM1-6 (Fig. 7). In this complex mutant, three DNA fragments were inserted into position 158–168 of the *gpt* gene, and the direction and the order of the inserted fragments were different from those of the original sequences. The original locations of fragment 1 (335 bp), fragment 2 (1092 bp), and fragment 3 (133 bp) were 17, 13, and 22 kbp, respectively, from the inserted position. A mutation in the control group of this class was a sequence substitution of 5′-CCG-3′ to 5′-ACC-3′ in position 278–280.

4. Discussion

Significant and dose-related increases in Spi$^-$ and *gpt* MFs of the GDL1 cells were observed after treatment with MMC (Fig. 2, Tables 1 and 2). In the in vivo experiment using *gpt* delta mice exposed to MMC [8], statistically significant increases of large deletion mutations (class I, Table 3) in Spi$^-$ mutants and tandem base substitutions at the 5′-GG-3′ or 5′-CG-3′ sequence (Table 4) in *gpt* mutants were seen. These mutations were also predominantly induced in GDL1 cells by MMC (Tables 3 and 4). In addition, MMC-induced complex mutations (class IV) in Spi$^-$ mutants and single base substitutions at G:C bp in the *gpt* mutants were observed in the GDL1 cells (Tables 3 and 4). Increase of these mutations was not observed in *gpt* delta mice treated with MMC [8]. Single base substitutions at G:C bp induced by MMC were also reported in another mammalian cell in vitro [25]. Monoadducts of MMC are probably responsible for single base mutations [26], and adducts are preferentially formed in the 5′-CG-3′ and 5′-GG-3′ sequences [23,24]. In fact, most of the single base substitutions were observed at guanines at the 5′-CG-3′ or 5′-GG-3′ sequences (Fig. 6). The GDL1 cell line was established from the genetic modification of introducing an artificially constructed expression unit for the SV40 T antigen gene into lung fibroblasts of *gpt* delta mice. The SV40 T antigen can immortalize fibroblasts through formation of complexes with p53 and interruption of p53-dependent growth suppression [27–29]. Hence, the normal function of p53 might be lost in the GDL1 cells.

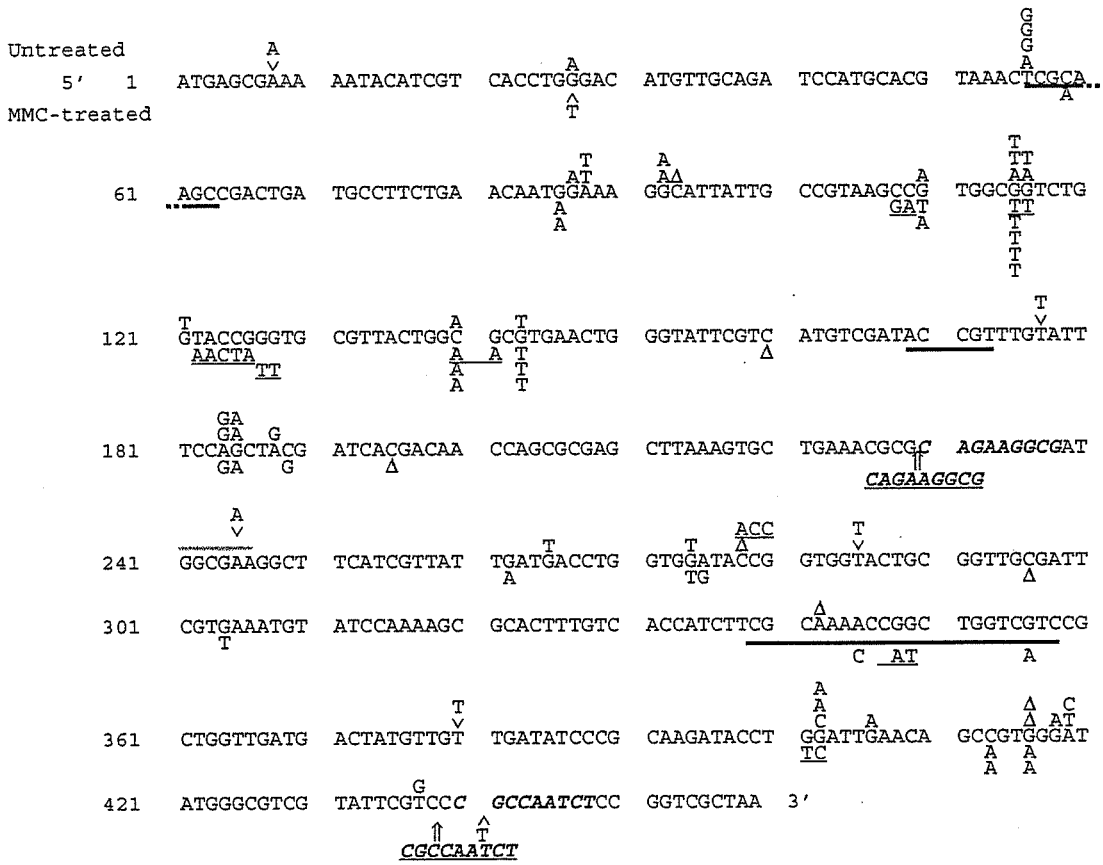

Fig. 6. Mutations in the *gpt* gene obtained from MMC-treated and untreated GDL1 cells. The sequence from top to the bottom represents the coding region of the *gpt* gene. Mutations shown above the sequence are from untreated cells and below from cells treated with MMC. (Δ and ∧) Single base deletions and one base insertion, respectively. Tandem base substitutions and sequence substitutions are underlined. Bars represent deleted sequences in deletion mutations. Inserted sequences are underlined and insertion positions are shown with arrows. The repeated sequences are shown in italicized boldface. In MMC-treated cells, a 329-bp deletion in nucleotide −3 to 326 (−3 indicates 3 bp prior to the first base of the first codon) and a 565-bp deletion accompanied by 1 bp insertion in position 11–575, and a complex rearrangement are not represented in Fig. 6 (see Fig. 7 for a complex rearrangement). One *gpt* mutant in untreated cells had two G:C to T:A mutations in nucleotide 121 and 143.

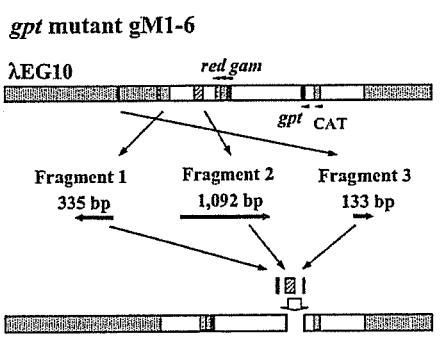

Fig. 7. Rearrangement induced in the *gpt* mutant derived from MMC-treated GDL1 cells. In *gpt* mutant gM1-6, three DNA fragments, fragment 1 (335 bp), fragment 2 (1092 bp), and fragment 3 (133 bp), were inserted into position of 158–168 of the *gpt* gene, and the directions and orders of the inserted fragments were different from that of the original sequence.

The p53 gene plays an important role in nucleotide excision repair (NER) [30–33] and NER activity decreased in cell lines transformed with the SV40 T antigen [34] and papillomavirus E6 genes [35]. Therefore, the potency of p53-dependent DNA repair pathways including NER might be different between GDL1 cells and *gpt* delta mice, which could account for the induction of single base substitutions and complex mutations (see below) in GDL1 cells.

Five complex mutations of Spi$^-$ (Fig. 5) and one rearranged mutant of *gpt* (Fig. 7) were observed in MMC-treated GDL1 cells. Comparison of the Spi$^-$ mutant in $p53^{+/+}$ and $p53^{-/-}$ *gpt* delta mice exposed to carbon-ion irradiation indicated that the induction of complex rearrangements was significantly accelerated by p53-knockout in the kidney, where p53 is highly expressed, but not in the liver, where p53 is weakly

Table 3
Comparison of specific MF of Spi⁻ mutations between *gpt* delta mice and GDL1 cells

Type of mutation	Class of mutation	Control			MMC			
		gpt delta mice[a]	GDL1 cells		*gpt* delta mice[a]		GDL1 cells	
		Specific MF[b] ($\times 10^{-6}$)	Specific MF[b] ($\times 10^{-6}$)	*P* value[c,d]	Specific MF[b] ($\times 10^{-6}$)	*P* value[c,e]	Specific MF[b] ($\times 10^{-6}$)	*P* value[c,f]
Large deletion (>1 kbp)								
With microhomology	I-A	0.0	4.2	<0.0001	1.6	<0.001	17.6	<0.01
Without microhomology	I-B	0.1	0.0	1.00	0.6	0.19	5.9	<0.05
Midsize deletion (2 bp to 1 kbp)	II	0.0	1.2	<0.05	0.2	0.47	7.8	<0.05
Single base deletion								
At run sequence	III-A	1.4	17.3	<0.0001	1.4	1.00	33.2	0.06
At non-run sequence	III-B	0.1	1.2	0.08	0.2	1.00	0.0	1.00
Complex mutation	IV	0.0	0.0	–	0.0	–	9.8	<0.001
Miscellaneous mutation	V	0.1	1.8	<0.05	1.3	<0.05	11.7	<0.01
Unidentified		0.0	0.0	–	0.0	–	2.0	0.24
Total		1.8	25.6	<0.0001	5.2	<0.01	88.0	<0.0001

[a] Data previously reported by us [8].
[b] Specific MF was calculated by multiplying the total mutation frequency by the ratio of each type of mutation to the total mutation.
[c] *P* values were determined using Fisher's exact test according to Carr and Gorelick [22].
[d] Comparison between the control group of *gpt* delta mice and control group of GDL1 cells.
[e] Comparison between the control group of *gpt* delta mice and MMC-treated group of *gpt* delta mice.
[f] Comparison between the control group of GDL1 cells and MMC-treated group of GDL1 cells.

expressed [36]. Thus, a p53 defect by the recombinant SV40 T antigen may cause the DNA rearrangement occurring in GDL1 cells. The breakage-fusion bridge cycle reported in p53 deficient mammalian cells might involve in the DNA rearrangement observed in GDL1 cells [37,38].

It is interesting and surprising to note that Spi⁻ mutant sM1-9 has a DNA fragment from chromosome

Table 4
Comparison of specific MF of *gpt* mutations between *gpt* delta mice and GDL1 cells

Type of mutation	Control			MMC			
	gpt delta mice[a]	GDL1 cells		*gpt* delta mice[a]		GDL1 cells	
	Specific MF[b] ($\times 10^{-6}$)	Specific MF[b] ($\times 10^{-6}$)	*P* value[c,d]	Specific MF[b] ($\times 10^{-6}$)	*P* value[c,e]	Specific MF[b] ($\times 10^{-6}$)	*P* value[c,f]
Base substitution/single							
At G:C	5.4	10.9	<0.05	6.6	0.47	40.3	<0.0001
At A:T	1.7	5.9	<0.01	1.9	0.75	5.3	1.00
Insertion	0.0	2.5	<0.01	0.0	–	7.0	0.12
Deletion	1.1	3.0	0.10	0.9	0.30	10.5	<0.05
Base substitution/tandem	0.0	0.0	–	3.3	<0.001	8.8	<0.001
Others	0.0	0.5	0.35	1.4	<0.05	7.0	<0.05
Total	8.2	22.7	<0.0001	14.1	<0.0001	78.9	<0.0001

[a] Data previously reported by us [8].
[b] Specific MF was calculated by multiplying the total mutation frequency by the ratio of each type of mutation to the total mutation.
[c] *P* values were determined using Fisher's exact test according to Carr and Gorelick [22].
[d] Comparison between the control group of *gpt* delta mice and control group of GDL1 cells.
[e] Comparison between the control group of *gpt* delta mice and MMC-treated group of *gpt* delta mice.
[f] Comparison between the control group of GDL1 cells and MMC-treated group of GDL1 cells.